

Chapter 2

Phase transitions in Antiferroelectric Liquid Crystals: A Theoretical Model

2.1 Overview

Organic compounds with rod like molecules forming liquid crystalline phases often carry permanent electric dipole moments with components parallel and/or perpendicular to the long axes of the molecules. Hence, one could expect ferroelectric properties in such liquid crystalline phases. Several theoretical considerations for the realization of a true ferroelectric liquid or the polar nematic phase have been reported. However, upto now there is no clear experimental evidence for such a polar nematic phase. On the other hand, using symmetry arguments, Meyer *et al.* [1] demonstrated that the C_2 point symmetry of the layers in the chiral smectic C (SmC^*) phase allows them to be polarized in the plane of the layers. As this transversely polarized SmC^* phase can have potential applications in display devices many compounds exhibiting SmC^* phase have been synthesized and the properties of this phase have been extensively studied [31].

As we have mentioned in Chapter 1, Chandani *et al.* [2] discovered transverse *antiferroelectricity* in the compound 4 - (1 - nlethylheptyloxycarbonyl) phenyl 4' - octylcarbonyloxybiphenyl - 4 - carboxylate (MHPOBC). Further detailed studies show that in addition to the antiferroelectric (SmC_A^*) phase, these novel compounds exhibit a rich variety of other phases as they are cooled from the isotropic phase:



where the symbol SmC_β^* denotes the usual ferroelectric SmC^* phase. The subscript β has been given to distinguish it from the other phases in these compounds. Though the structures of SmC_β^* and SmC_A^* phases are well understood as discussed in chapter 1, the structures of SmC_α^* and SmC_γ^* phases are not clearly elucidated. Several experimental studies using a variety of techniques have established the following facts:

- All the tilted phases have a helical structure and it is established by optical measurements that the sense of the helix is opposite in SmC_β^* and SmC_A^* phases [8].

- All the transitions between different tilted phases are *weakly* first order in nature as determined by differential scanning calorimetry (DSC) with heats of transition ≈ 1 joule/mole [9].
- The SmC_γ^* phase is *ferrielectric* in nature as the effective polarization in this phase is lower than that in the SmC_β^* phase. Several pure compounds exhibit two ferri phases [33] whereas in some binary mixtures there are three sub-phases FI_H , SmC_γ^* and FI_L [6].
- The ferrielectric phase has a rather turbid appearance with in-plane birefringence rendering optical measurements in this phase difficult [33, 10].
- Optical and x-ray measurements reveal that the SmC_α^* phase has a small tilt angle and a very short pitch [6, 7]. Also this phase has ferrielectric characteristics at lower temperatures but antiferroelectric characteristics close to the SmA-SmC_α^* transition temperature [12, 13].
- The stability of the SmC_α^* and ferrielectric phases is sensitive to the optical purity of the sample. The temperature ranges of stability of these phases decrease and finally go to zero when the compound is mixed with its opposite handed enantiomer [6]. The range of SmC_α^* phase shrinks as the nonchiral chain length is increased [9].
- Studies on several homologous series have shown a prominent *odd-even* effect in the phase transition temperatures between the SmC_β^* to SmC_γ^* as well as SmC_γ^* to SmC_A^* phases [9].
- A strong transverse dipolar group attached close to the chiral center favours the formation of the SmC_A^* phase. However, even racemic mixtures with zero polarization [6] and achiral compounds [11] also exhibit the *anticlinic* phase in which successive layers have opposite tilts.
- The apparent tilt angle (the angle between the effective optical axis of the field distorted structure and the layer normal) measurements on homogeneously aligned samples revealed that in the SmC_α^* phase, there is a step like variation of the apparent tilt angle as a function of an in-plane external static electric field [14]. This led to the speculation that there is a field induced *devil's staircase* in this phase.
- The variation of the apparent tilt angle with the applied dc electric field in the ferrielectric phase exhibits a plateau at one third of the tilt angle at intermediate fields [14].
- The conoscopic figures obtained from thick homeotropically aligned samples also show distinct characteristic changes as a function of an in-plane external static electric field in the ferrielectric [15] and SmC_α^* [14] phases. In both of these phases the conoscopic figure of the uniaxial medium at zero field acquires biaxial characteristics with the optic axial plane *parallel* to the electric field at intermediate fields which then switches to the *orthogonal* direction beyond a critical field [15, 14].

Several phenomenological theories have been developed to account for some of the above experimental observations in these compounds. In these phenomenological Landau type

theories one expands the free energy density in powers of suitable order parameters to describe the transitions between the phases.

The first theory of this type for antiferroelectric liquid crystals was developed by Orihara *et al.* [16]. They assumed bilayer order in the ferro, ferri and antiferro phases to define the order parameters which vary continuously along the layer normal. To a first approximation, neglecting the fluctuations or *inhomogeneous* terms of the free energy density expansion, they obtained transitions between the ferro, ferri and antiferroelectric phases. Later Lorman *et al.* [17] extended this model to include the inhomogeneous terms in the free energy density expansion. However, these continuum theories do not account for the SmC_α^* phase. Further, experimental observations [6, 10] in the ferroelectric phase appear to indicate that this phase has multi-layer order and the assumed bilayer order may not be adequate in this phase.

To improve upon this, a discrete model taking into account the configuration of each layer was first proposed by Sun *et al.* [34]. Later treating the configuration of each layer as an Ising variable, Yamashita *et al.* [18, 19] developed a model in analogy with *Axial Next Nearest Neighbour Ising* (ANNNI) model taking into account upto third nearest neighbour interactions. Again both these discrete models do not account for the SmC_α^* phase. In the Ising picture, the helicoidal structures which are present in all the tilted phases have been neglected.

In order to account for the SmC_α^* phase and the experimental observations mentioned above, we developed a discrete phenomenological model [35] for this system by including NN as well as competing NNN interactions between the layers whose origins are also discussed in Sec 2.4.1. In our theory, the configuration of each layer is described by a 2-d axial vector as in [34] and hence the resulting model is of xy-type. Our model takes into consideration the helicoidal structures of the phases and accounts for the SmC_α^* as well as the three ferroelectric phases often seen in these systems.

In Sec. 2.2, we will describe the continuum theories developed for this system in earlier studies which form a theoretical background to our model. In Sec. 2.3 we will consider other models *viz.* the Ising type models often invoked for this system. In this section we will also point out the shortcomings of these models. Then in Sec. 2.4, we will discuss the discrete model developed by us. Finally the main conclusions of this chapter will be summarized in Sec. 2.5.

2.2 Continuum theory of AFLC

In the uniaxial SmA phase as the long axes of the cylindrical rod like molecules orient on average along the layer normal, they can rotate freely about their long axes. But in the tilted smectic phases, the tilt order induces a hindrance to this free rotation. If the net dipole moment of such a molecule has a component perpendicular to the long axis of the molecule then one can expect the layers to become transversely polarized. However, in the SmC phase made of *achiral* molecules, the symmetry C_{2h} of the layers contain a mirror plane perpendicular to the C_2 axis and the above rotational bias can only produce quadrupolar order within the layers. But, if the molecules are *chiral*, this mirror plane perpendicular to the C_2 axis is removed and the layers in the resulting SmC^* phase become

transversely polarized. As this transverse polarization is a consequence of the tilt order of the layers, the latter is taken as the primary order parameter whereas the former is a secondary order parameter [31] in the theories described below.

2.2.1 Order parameters

A complete prescription of the "order" in one of the tilted smectic phases involves many elements: (a) The orientational order of the rod like molecules implicitly assumed to be perfect and represented only by the director \mathbf{A} (b) The one dimensional translational order which can be described by the density wave $\psi = |\psi| \exp[i(\vec{k} \cdot \vec{r} + a)]$, where $|\psi|$ is the amplitude, α is an arbitrary initial phase and \vec{k} is the wave vector. Again $|\psi|$ is implicitly assumed to be a constant and in effect only the magnitude of \vec{k} which is coupled to the tilted orientation of the molecules within the layers is taken into account. (c) The tilt order of the director \hat{n}_i in the i -th layer which can be described by an axial vector $\vec{\xi}_i$ defined as

$$\vec{\xi}_i = (\hat{n}_i \cdot \hat{k})(\hat{n}_i \times \hat{k}). \quad (2.1)$$

Note that the definition is consistent with the apolar nature of the director \mathbf{A} .

Assuming that the wave vector \vec{k} is parallel to the z -axis, the order parameter to within an arbitrary constant is then

$$\vec{\xi}_i = (n_{iy}n_{iz}, -n_{ix}n_{iz}) \propto \frac{\sin 2\theta_i}{2} (\sin \phi_i, -\cos \phi_i), \quad (2.2)$$

where n_{ix} , n_{iy} and n_{iz} are the Cartesian components of \hat{n}_i . Note that $\vec{\xi}_i$ is perpendicular to the c -vector \vec{c}_i of the i -th layer as shown in Fig. 2.1. In the ferroelectric phase $\vec{\xi}_i$ and the corresponding \vec{P}_i are the only order parameters which are assumed to be continuous functions of x . Detailed theoretical models using these order parameters have been developed to account for the various physical properties of this phase [31].

In the *antiferroelectric* phase the angle between the c -directors of successive layers is close to π and it is convenient to define two primary order parameters $\vec{\xi}_a$ and $\vec{\xi}_f$ as

$$\vec{\xi}_a = (\vec{\xi}_1 - \vec{\xi}_2)/2 \quad (2.3)$$

$$\vec{\xi}_f = (\vec{\xi}_1 + \vec{\xi}_2)/2, \quad (2.4)$$

where $\vec{\xi}_1$ represents the orientations of the molecules in the odd-numbered layers and $\vec{\xi}_2$ those for the nearest neighbour even-numbered layers along the positive z -axis. The subscripts "a" and "f" represent antiferroelectric and ferroelectric order respectively. Similarly the secondary order parameters \vec{P}_a and \vec{P}_f are defined as

$$\vec{P}_a = (\vec{P}_1 - \vec{P}_2)/2 \quad (2.5)$$

$$\vec{P}_f = (\vec{P}_1 + \vec{P}_2)/2, \quad (2.6)$$

where \vec{P}_1 and \vec{P}_2 are the polarizations in the neighbouring layers as defined above. These order parameters are assumed to vary sufficiently slowly along the layer normal to treat them as continuous functions of x .

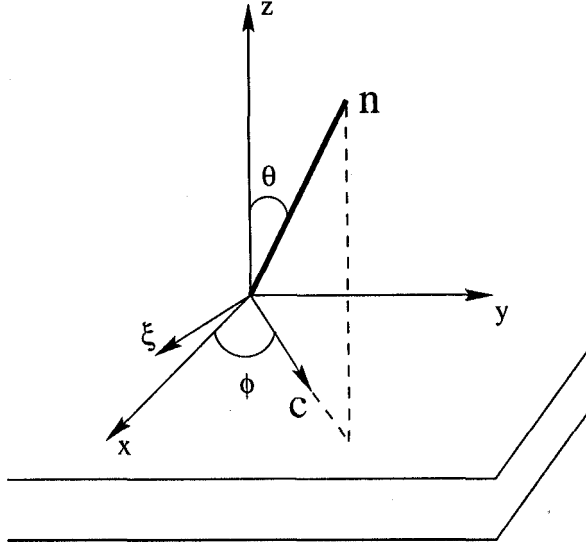


Fig. 2.1: The definition of order parameter for a smectic layer.

Though all these variables transform like vectors under all rotations of the symmetry group D_2 , the antiferroelectric and ferroelectric variables transform in different ways under translation. \vec{P}_a changes sign under a translation parallel to the layer normal by a layer spacing while \vec{P}_f does not change. Hence, if the smectic liquid crystal is regarded as a one dimensional crystal, then \vec{P}_f and \vec{P}_a are the zone center and zone boundary modes respectively.

Neglecting the in-plane fluctuation of the order parameters the free energy density can now be expanded in terms of these order parameters and their derivatives along the z-axis. In Sec. 2.2.2 we will consider the homogeneous case neglecting the terms involving the derivatives of the order parameters following the discussion by Orihara et al. [16]. The inhomogeneous case including the derivative terms will be discussed in Sec. 2.2.3 as was first considered by Lorman et al. [17].

2.2.2 Homogeneous case

The homogeneous part of the free energy density consistent with the symmetry (*viz.* D_2) of the high temperature SmA phase can be expanded as

$$\begin{aligned} \mathcal{F}_{hom} = & \frac{\alpha'_a}{2} \xi_a^2 + \frac{\alpha'_f}{2} \xi_f^2 + \frac{\beta_a}{4} \xi_a^4 + \frac{\beta_f}{4} \xi_f^4 + \frac{\gamma_1}{2} \xi_a^2 \xi_f^2 + \frac{\gamma_2}{2} (\vec{\xi}_a \cdot \vec{\xi}_f)^2 \\ & - \lambda_a \vec{\xi}_a \cdot \vec{P}_a - \lambda_f \vec{\xi}_f \cdot \vec{P}_f + \frac{1}{2\chi_a} P_a^2 + \frac{1}{2\chi_f} P_f^2 - \vec{E} \cdot \vec{P}_f, \end{aligned} \quad (2.7)$$

where $\xi_{a(f)} = |\vec{\xi}_{a(f)}|$ and \vec{E} is the external field. Terms upto 4-th order in the primary order parameters $\vec{\xi}_{a(f)}$ and upto 2nd order in secondary order parameters $\vec{P}_{a(f)}$ are retained in the expansion. As is usual in a Landau theory one can assume that the coefficients α'_a and α'_f are temperature dependent with $\alpha'_a = A(T - T_c)$ and $\alpha'_f = \alpha'_a + 6$. The terms with

coefficients A , and λ_f are called *electroclinic* terms which are analogous to the *piezoelectric* terms in solid state physics. These two terms are *pseudo scalar* and are allowed only in a *chiral* medium. The terms with χ_a and χ_f are of entropic origin arising from the rotational degrees of freedom of the tilted molecules about their long axes [31]. The last term is the coupling of electric field with the polarizations of the layers.

Minimization of Eq. 2.7 with respect to \vec{P}_a and \vec{P}_f and eliminating the two, the free energy density using polar coordinates can be written as

$$\mathcal{F}_{hom} = \frac{\alpha_a}{2}\xi_a^2 + \frac{\alpha_f}{2}\xi_f^2 + \frac{\beta_a}{4}\xi_a^4 + \frac{\beta_f}{4}\xi_f^4 + \frac{\gamma_1}{2}\xi_a^2\xi_f^2 + \frac{\gamma_2}{2}\xi_a^2\xi_f^2\cos^2\Phi - E'\xi_f\cos\Psi, \quad (2.8)$$

where $\alpha_{f(a)} = \alpha'_{f(a)} - \chi_{f(a)}\lambda_{f(a)}^2$. The angle between $\vec{\xi}_a$ and $\vec{\xi}_f$ and that between \vec{E} and $\vec{\xi}_f$ are Φ and Ψ respectively. The equilibrium and stability conditions for Φ and Ψ are

$$\frac{\partial\mathcal{F}_{hom}}{\partial\Phi} = -\frac{\gamma_2}{2}\xi_a^2\xi_f^2\sin 2\Phi = 0, \quad (2.9)$$

$$\frac{\partial\mathcal{F}_{hom}}{\partial\Psi} = E'\xi_f\sin\Psi = 0, \quad (2.10)$$

$$\frac{\partial^2\mathcal{F}_{hom}}{\partial\Phi^2} = -\gamma_2\xi_a^2\xi_f^2\cos 2\Phi > 0, \quad (2.11)$$

$$\frac{\partial^2\mathcal{F}_{hom}}{\partial\Psi^2} = E'\xi_f\cos\Psi > 0. \quad (2.12)$$

From Eqs. 2.9-2.12 stable equilibrium solutions are $\Phi = 0$ or π if $\gamma_2 < 0$ and $\Phi = \pi/2$ if $\gamma_2 > 0$, and $\vec{\xi}_f$ is always parallel to \vec{E} i.e., $\Psi = 0$.

Now Eq. 2.8 can be expressed in terms of the amplitudes ξ_a and ξ_f as

$$\mathcal{F}_{hom} = \frac{\alpha_a}{2}\xi_a^2 + \frac{\alpha_f}{2}\xi_f^2 + \frac{\beta_a}{4}\xi_a^4 + \frac{\beta_f}{4}\xi_f^4 + \frac{\gamma}{2}\xi_a^2\xi_f^2 - E'\xi_f, \quad (2.13)$$

where $\gamma = \gamma_1 + \gamma_2\cos^2\Phi$ and Φ can take values (0 or π) or $\pi/2$ depending on the sign of γ_2 . Minimization of Eq. 2.13 with respect to ξ_a and ξ_f in absence of the external electric field stabilize the five low symmetry phases. These are defined by the following equilibrium values of the order parameters

I. $\xi_a = 0, \xi_f^2 = \frac{-\alpha_f}{\beta_f};$

II. $\xi_a^2 = \frac{-\alpha_a}{\beta_a}, \xi_f = 0;$

III and IV. $\xi_a^2 = \frac{-\alpha_a\beta_f + \gamma\alpha_f}{\beta_a\beta_f - \gamma^2}, \xi_f^2 = \frac{-\alpha_f\beta_a + \gamma\alpha_a}{\beta_a\beta_f - \gamma^2}, \Phi = 0$ or $\pi;$

V. $\xi_a^2 = \frac{-\alpha_a\beta_f + \gamma\alpha_f}{\beta_a\beta_f - \gamma^2}, \xi_f^2 = \frac{-\alpha_f\beta_a + \gamma\alpha_a}{\beta_a\beta_f - \gamma^2}, \Phi = \pi/2;$

The smectic ordering corresponding to the preceding equilibrium values of the order parameter are represented in Fig. 2.2. One can see that three types of dipolar orders are possible. Fig. 2.2a represents the ferroelectric mono-layer ordering with the polarizations

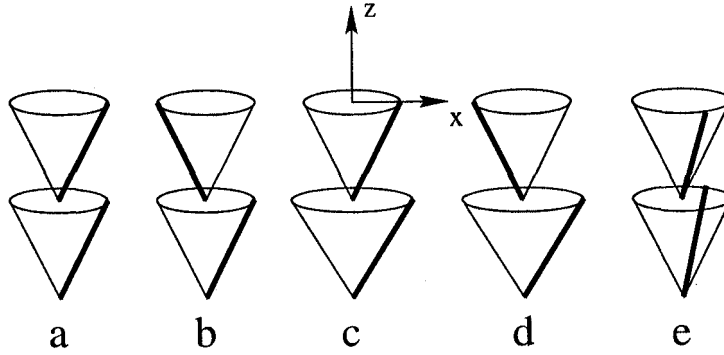


Fig. 2.2: The bilayer structures of different phases predicted by homogeneous model.

(\vec{P}) remaining parallel in successive layers. Fig. 2.2b corresponds to an antiferroelectric bilayer ordering, with an antiparallel orientation for adjacent \mathbf{P} vectors. Fig. 2.2c-2.2e represent the three types of ferroelectric ordering, which can be distinguished by their tilt and azimuthal angles. Thus Fig. 2.2c & 2.2d represent ferroelectric structures in which two adjacent layers possess different tilt angles and the difference in azimuthal angle is 0 and π respectively. In the structure shown in Fig. 2.2e the molecules in successive layers have the same tilt angles but different arbitrary azimuthal angles. As one can guess the structures shown in Fig. 2.2c and 2.2d for the ferroelectric phase involve changes in the layer spacing from layer to layer and are energetically not favoured. In fact x-ray studies have not found any evidence for these structures in the ferroelectric phase. Orihara et al. [16] have constructed the phase diagram representing the various types of phase sequences predicted by their model in the $\beta_a - \beta_f$ plane without going into the detailed structure of the ferroelectric phase.

2.2.3 Inhomogeneous case

In Sec. 2.2.2 only a homogeneous form of the free energy density was considered. Taking into account the influence of the chiral symmetry of the molecules to produce a helicoidal structure along the z-axis the total free energy density \mathcal{F} is a sum of two parts

$$\mathcal{F} = \mathcal{F}_{hom} + \mathcal{F}_{inh} \quad (2.14)$$

where the \mathcal{F}_{hom} is given by Eq. 2.7 and \mathcal{F}_{inh} is the inhomogeneous part of the free energy density. Assuming that there is no variation of the orientational order parameters within the smectic layers, extending the method used for ferroelectric liquid crystals [31], \mathcal{F}_{inh} can be written as [16]

$$\begin{aligned} \mathcal{F}_{inh} = & \delta_a \left(\xi_{ax} \frac{d\xi_{ay}}{dz} - \xi_{ay} \frac{d\xi_{ax}}{dz} \right) + \delta_f \left(\xi_{fx} \frac{d\xi_{fy}}{dz} - \xi_{fy} \frac{d\xi_{fx}}{dz} \right) \\ & + \mu_a \left(P_{ax} \frac{d\xi_{ay}}{dz} - P_{ay} \frac{d\xi_{ax}}{dz} \right) + \mu_f \left(P_{fx} \frac{d\xi_{fy}}{dz} - P_{fy} \frac{d\xi_{fx}}{dz} \right) + \\ & \frac{\kappa_a}{2} \left(\frac{d\xi_a}{dz} \right)^2 + \frac{\kappa_f}{2} \left(\frac{d\xi_f}{dz} \right)^2 \end{aligned} \quad (2.15)$$

where the first two terms with coefficient b , and δ_f are the lowest order *Lifshitz* invariants allowed by the chiral symmetry of the medium. The terms with coefficients μ_a and μ_f are the *flexoelectric* terms and the last two are the usual elastic energies associated with the distortions of the director.

Lorman *et al.* [17] assumed that the tilt order of the smectic is homogeneous (*i.e.*, θ is independent of z). This is a reasonable approximation in tilted smectic liquid crystals far from the SmA-SmC transition point and in the absence of an external field. The distortions in the tilt angle (the so called *soft mode*) which involves changes in layer spacing is energetically less favoured compared to distortions in the azimuthal angle (the *Goldstone mode*). Then from Eq. 2.2-2.4, the order parameters $\vec{\xi}_a$ and $\vec{\xi}_f$ become

$$\vec{\xi}_a = \xi_o(-\sin \psi \sin \phi, \sin \psi \cos \phi), \quad (2.16)$$

$$\vec{\xi}_f = \xi_o(-\cos \psi \cos \phi, \cos \psi \sin \phi), \quad (2.17)$$

where the variables ξ_o , ϕ and ψ are given by

$$\xi_o = \frac{\sin 2\theta}{2}, \quad \phi = \frac{\phi_2 + \phi_1}{2}, \quad \psi = \frac{\phi_2 - \phi_1}{2}. \quad (2.18)$$

Now using the expressions for $\vec{\xi}_a$ and $\vec{\xi}_f$ from Eq. 2.16 and Eq. 2.17 and including ξ_o in the phenomenological coefficients, the free energy per unit area in the absence of electric field takes the form

$$\begin{aligned} &= \int \left[\frac{1}{2} \left(\frac{d\phi}{dz} \right)^2 (\kappa^+ + \kappa^- \cos 2\psi) + \frac{1}{2} \left(\frac{d\psi}{dz} \right)^2 (\kappa^+ - \kappa^- \cos 2\psi) \right. \\ &\quad \left. - \left(\frac{d\phi}{dz} \right) (\delta^+ + \delta^- \cos 2\psi) + \frac{a_1}{2} \cos 2\psi + \frac{b_1}{4} \cos^2 2\psi \right] dz \end{aligned} \quad (2.19)$$

where $\kappa^+ = (\kappa_f + \kappa_a)/2$, $\kappa^- = (\kappa_f - \kappa_a)/2$, $\delta^+ = -(\delta_f + \delta_a)/2 - (\lambda_f \chi_f \mu_f + \lambda_a \chi_a \mu_a)/2$, $\delta^- = -(\delta_f - \delta_a)/2 - (\lambda_f \chi_f \mu_f - \lambda_a \chi_a \mu_a)/2$, $a_1 = \alpha_f/2 - \alpha_a/2 + \beta_f/4 - \beta_a/4$ and $b_1 = \beta_f/4 + \beta_a/4 - \gamma_1/8$. Note that there is a linear term in $d\phi/dz$ in Eq. 2.19 which stabilizes a spontaneous helicoidal structure. This term vanishes in a non-chiral medium as δ^+ and δ^- are zero in such a medium.

From the Euler-Lagrange equations corresponding to the variation of ϕ and ψ in the free energy functional Eq. 2.19, we get

$$(\kappa^+ + \kappa^- \cos 2\psi) \frac{d\phi}{dz} - (\delta^+ + \delta^- \cos 2\psi) = C, \quad (2.20)$$

$$\begin{aligned} (\kappa^+ - \kappa^- \cos 2\psi) \frac{d^2\psi}{dz^2} &= \kappa^- \sin 2\psi \left(\frac{d\phi}{dz} \right)^2 - \kappa^- \sin 2\psi \left(\frac{d\psi}{dz} \right)^2 \\ &\quad + 2\delta^- \sin 2\psi \frac{d\phi}{dz} - a_1 \sin 2\psi - b_1 \sin 2\psi \cos 2\psi, \end{aligned} \quad (2.21)$$

where C is the first integral value that depends on the external parameters. It is easy to see that a stable solution of Eq. 2.20 and Eq. 2.21 corresponds to a uniform helicoidal structure with

$$\phi = kz, \quad \psi = \text{const.}, \quad (2.22)$$

where k is the wave vector of the helix. k and ψ do not depend on z but vary with the external variables. In other words, one obtains an in-phase azimuthal angle ϕ that depends linearly on z , whereas the azimuthal anti-phase angle ψ is independent of the z variable.

Substituting the stable solutions Eq. 2.22 in the Landau-Ginzburg potential Eq. 2.19, one gets by integrating with respect to the z variable,

$$F(k, \psi) = \left[\frac{k^2}{2} (\kappa^+ + \kappa^- \cos 2\psi) + k(\delta^+ + \delta^- \cos 2\psi) + \frac{a_1}{2} \cos 2\psi + \frac{b_1}{4} \cos^2 2\psi \right], \quad (2.23)$$

which is a simple algebraic expression. The different phases correspond to different values of the anti-phase azimuthal angle ψ .

According to this model, in the ferrielectric SmC_γ^* phase, the difference in azimuthal angles between a pair of near neighbour layers *i.e.*, ψ is fixed at a value between 0 and π , such pairs in turn having a helical arrangement. The two limiting angles correspond to ferro- and antiferro- phases respectively. The phase diagrams corresponding to different values of the phenomenological coefficients have been calculated in Ref. [17]. Note that both the ferro- and antiferroelectric phases predicted by this model are different from the experimentally exhibited structures as ψ within a unit cell is exactly 0 and π in the two predicted phases respectively. Further, the field induced structural changes can not be studied using this approximation. It has been pointed out by Gorecka *et al.* [15] that this type of model can not explain the conoscopic observations in the ferrielectric phase in the presence of a field (see chapter 4 for details).

2.3 Other relevant models

From the switching current measurements in the SmC_α^* phase, Takanishi *et al.* [13] found that this phase has antiferroelectric characteristics close to the $\text{SmA} - \text{SmC}_\alpha^*$ transition temperature but acquires ferrielectric characteristics with decreasing temperature. Hiraoka *et al.* [14] performed apparent tilt angle measurements in the SmC_α^* phase as a function of the applied dc field. They found step like variation of the apparent tilt angle with increasing dc field. From these observations, they speculated the existence of a temperature induced as well as field induced devil's staircases in the SmC_α^* phase. Further, in the ferrielectric range, the apparent tilt angle measurements show a plateau at one third of the tilt angle at intermediate fields. This plateau indicates a field induced 1:2 structure ($/\backslash \backslash \dots$) in this phase. Conoscopic observations by Gorecka *et al.* [15] also indicate this field induced structure in the ferrielectric range. Later from conoscopic observations, Isozaki *et al.* [36, 37] have speculated that a temperature induced devil's staircase can be invoked in the ferrielectric range of AFLC also. Such a devil's staircase has been predicted using some Ising models. Bak *et al.* [38] have shown that the ground state of a system of Ising spins arranged in a 1-d lattice can exhibit a complete devil's staircase as a function of the field provided the interaction between the spins is long range and convex. The devil's staircase obtained by Bak *et al.* [38] for an antiferromagnetic inverse square interaction *viz.* $J(i) = i^{-2}$ is shown in Fig. 2.3. q along the y-axis represents the fraction of up spins

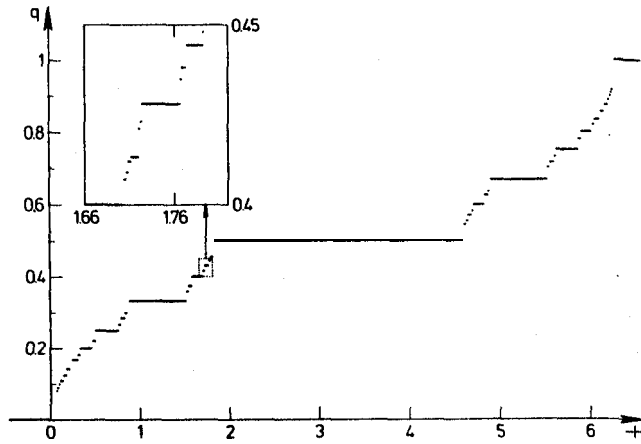


Fig. 2.3: Field induced devil's staircase exhibited by 1-d Ising model with long range convex interactions ($J(i) = i^{-2}$). After Ref. [38].

in a period. It can be noted that there is a wide plateau corresponding to antiferroelectric structures *i.e.*, $q = 0.5$ in this staircase.

Another model which exhibits temperature induced devil's staircase is the Axial Next Nearest Neighbour Ising or ANNNI model [20, 39]. In the 3D version of the model, Ising spins lying in a certain plane are coupled ferromagnetically to its z_0 nearest neighbours ($J_0 > 0$) while spins lying in different planes interact through nearest (J_1) and next nearest (J_2) neighbour competing interactions. The mean field phase diagram of the 3-d ANNNI model for $J_1 > 0$ is shown in Fig. 2.4. The structures $\langle k_1 k_2 \dots k_n \rangle$ represent the k-bands present in a period. A k-band is defined as the number of layers with parallel spins separated on both sides by oppositely oriented spins. Thus $\langle 2 \rangle$ represents $\uparrow\uparrow\downarrow\downarrow \dots$ structure, $\langle 12 \rangle$ represents $\uparrow\uparrow\downarrow \dots$ structure etc. The stable structures corresponding to negative J_1 can be obtained from that of positive J_1 by reversing every alternate spin. The structure $\langle 3 \rangle$ corresponding to positive J_1 becomes $\langle 12 \rangle$ for negative J_1 . With this transformation, the phase diagram corresponding to negative J_1 is the same as that for positive J_1 (see Selke [39] for a review). Thus the stability range of $\langle 3 \rangle$ phase for positive J_1 corresponds to the stability range of the $\langle 12 \rangle$ phase for negative J_1 . From the phase diagram, apart from ferro and antiferro phases we see three 'broad' phases namely $\langle 3 \rangle$ and $\langle 2 \rangle$ for $J_1 > 0$, $\langle 2 \rangle$ and $\langle 12 \rangle$ for $J_1 < 0$. Among these the stability range of $\langle 2 \rangle$ phase is rather wide as J_1 is varied.

The extension of the ANNNI model including a third neighbour interaction which was specifically used for describing liquid crystalline phases also exhibits similar structures. The mean field phase diagram of this model with $J_1 < 0$ is shown in Fig. 2.5. This model appears to widen the $\langle 12 \rangle$ range compared to that in Fig. 2.4.

Coming back to the AFLC system, to qualitatively account for the devil's staircase in the SmC_α^* phase, Takanishi et al. [13] invoked the Ising model developed by Bak et al. [38] treating the configuration of each layer as an Ising variable. Later to account for the temperature devil's staircase in the ferroelectric range, Yamashita et al. [18] (mistakenly)

SECTION 2.3

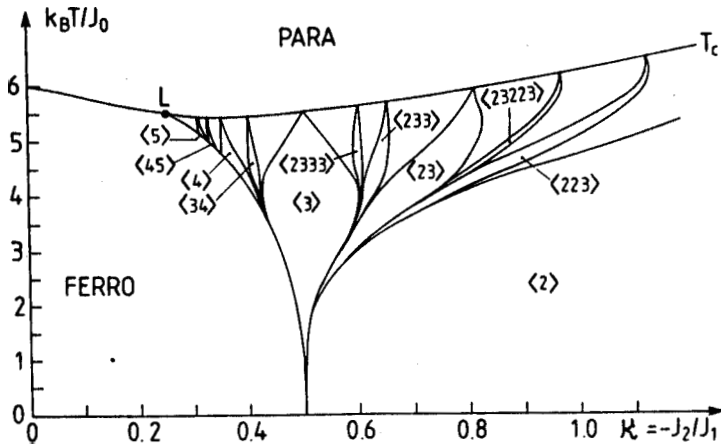


Fig. 2.4: Mean-field phase diagram of the 3-d ANNNI model showing some of the main commensurate phases. After Ref. [20]

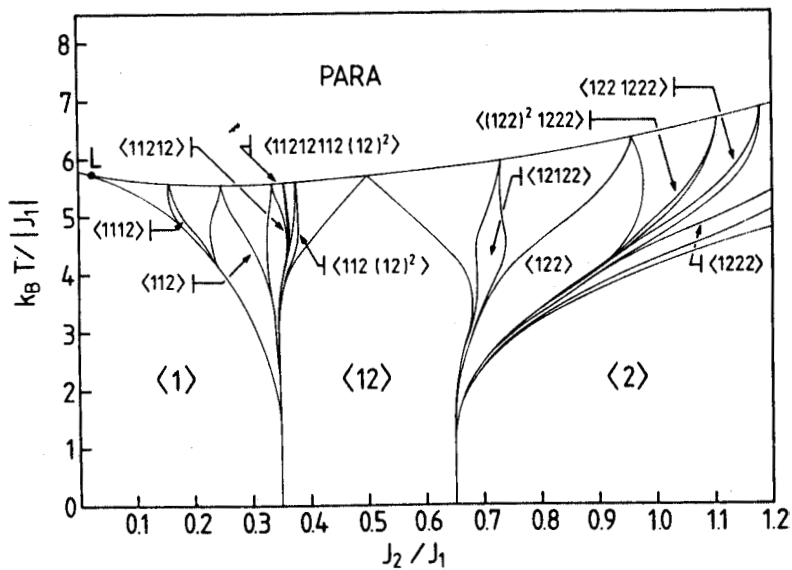


Fig. 2.5: Mean-field phase diagram of the ANNNI² model with third neighbour interaction for $J_0 = -J_1 > 0$ and $J_3 / J_0 = 0.1$, showing some of the main commensurate phases. After Ref. [20].

stated that the ANNNI model is not sufficient in this case as it does not stabilize the $\langle 12 \rangle$ (equivalent of 1:2 structure) which is seen in the presence of field. Therefore they extended the ANNNI model with third neighbour interaction, as stated above.

In the magnetic systems crystal fields confine the spins to specific orientations. In liquid crystals the polarization vectors are associated with liquid layers and indeed can align along any azimuthal direction to minimize the energy. As such, we believe that the Ising models are highly inappropriate for AFLC. This is further corroborated by the following facts:

1. From the conoscopic observations it is unequivocally established that all the tilted phases in the absence of field have helicoidal structures of \hat{n} along the layer normal. The assumption of the Ising character of the orientational order parameter is contrary to this helicoidal structure.
2. It is well known from the theory of ferroelectric phase (which is also a sub-phase exhibited by AFLC) that the order parameter is a 2-d vector in the plane of the layers, thus indicating xy- rather than Ising- character of the order parameters.
3. Both dielectric and electrooptic measurements detect modes with the relaxation frequencies typical of the Goldstone mode (involving the phase fluctuation of the orientation order parameter). This indicates an xy-type behaviour of the orientational order parameter in these phases.
4. Further even if we assume the ANNNI description as valid, it can be seen from the phase diagram of these models (Fig. 2.4 and 2.5) that as J_1 varies from large positive values in the ferroelectric phase through zero to large negative values in the antiferroelectric phase, the $\langle 22 \rangle$ structure has a large range of stability. However, experimentally this 4-layer antiferroelectric phase is not found in most of the pure compounds and even if it is found in some binary mixtures, it has very short temperature range of stability [6].
5. The ellipsometric studies by Bahr *et al.* [6] have not found any evidence for the 1:2 structure which is predicted by these Ising models to be the structure of the ferroelectric SmC_γ^* phase in the absence of a field.

More seriously none of the above models *i.e.*, both xy- and Ising- models account for the entire sequence of phases, particularly the SmC_α^* phase. We therefore developed an xy-type model taking into account the correct symmetry of the SmC^* layers. The pitch in some phases is found to be extremely short. Further, a field induced structure in the ferroelectric phase indicates a 3-layer periodicity. In contrast to the models described in Sec. 2.2, we do not assume a continuous variation of the order parameter along the layer normal and instead, we develop a discrete model. In the following, we will describe the model which accounts for the entire sequence of phases exhibited by AFLC.

2.4 Discrete model of AFLC

The experimental observations [7] of very short pitch in SmC_α^* phase indicate that the assumption of sufficiently slowly varying order parameters along the layer normal may

SECTION 2.4

not be appropriate. Therefore a model with the free energy density depending on the configuration of each layer is more relevant. Cepic *et al.* [40] first pointed out that second neighbour competing antiferroelectric coupling can lead to small pitch values as seen in the SmC_α^* phase in such a model.

This type of discrete model was first studied by Sun *et al.* [34]. However, they neglected the helicoidal structure which is present in all the tilted phases and assumed that in the SmC_γ^* phase, successive layers have opposite tilts of *different* magnitudes. But x-ray investigations in this phase have not found any evidence for this structure.

For molecules within a layer the anisotropic intermolecular dispersion interactions between the cores and end groups of the molecules as well as the packing considerations favour them to be parallel to one another. This gives rise to a strong ferroelectric coupling *within* the layers. On the other hand, for molecules in different layers, the interactions are mainly through end groups of the molecules or some long range interactions and are expected to be relatively weak. Therefore in the discrete model, we will assume that the tilt order within the smectic layers arise due to *intra-layer* interactions and such tilted layers are coupled *weakly* through nearest neighbour (NN) and next nearest neighbour (NNN) interactions.

In the following, we will consider different possible origins of such inter-layer interactions on the basis of which we will construct the free energy density expression of our model.

2.4.1 Origin of inter-layer interactions

As the layers are polarized, the most obvious candidate to give rise to an antiferroelectric NN interaction may seem to be dipolar coupling between the layers. However, Bruinsma *et al.* [21] pointed out that the dipolar coupling between i -th and j -th layers $V_{dp}(i-j)$, can be computed by treating each layer as a two dimensional liquid of dipoles. The interaction between two such layers separated by a distance d is

$$\begin{aligned} V_{dp}(i-j)/A &= S_i S_j \frac{P^2}{2\epsilon} \int d^2\rho \left[\frac{1}{(\rho^2 + d^2(i-j)^2)^{3/2}} - 3 \frac{(\vec{p} \cdot \hat{y})^2}{(\rho^2 + d^2(i-j)^2)^{5/2}} \right] \\ &= 0 \end{aligned} \tag{2.24}$$

where A is the area of the layer and $S_i P$ is the dipole moment per unit area of the i -th layer (along the y -axis). The cancelation is strict only in the thermodynamic limit of infinite A and is a consequence of Maxwell's law that an infinite slab of material, which is uniformly polarized perpendicular to the surface normal, has no electrical field outside the surface.

Therefore the antiferroelectric configuration is often thought to arise from dipolar interactions between a *pair of molecules* in adjacent layers [6]. However a simple calculation shows that this energy is much lower than the thermal energy and such pairs are unlikely to be important for the stability of the SmC_A^* phase.

The anisotropic dispersion interaction between tilted molecules in adjacent layers is minimized when the molecules in the two layers are in one plane. This gives rise to the two-fold anisotropic J_2 term in Eq. 2.30 below. Further, the dispersion interaction between

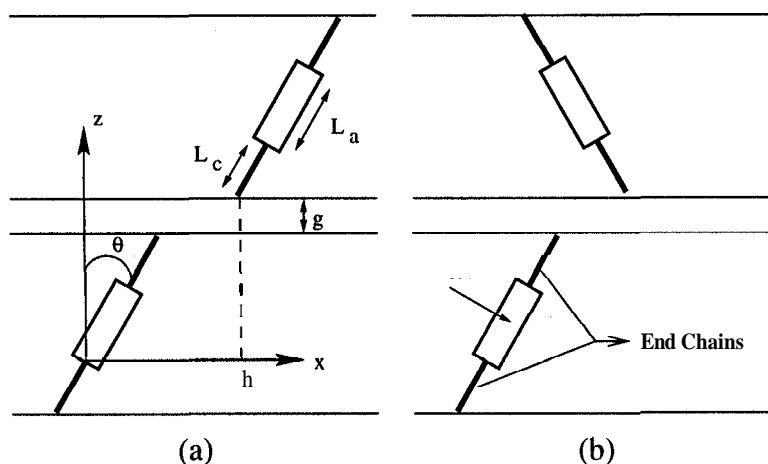


Fig. 2.6: The geometry for the calculation of dispersion interaction between the molecules.

the end chains of a pair of molecules in adjacent layers in ferroelectric and antiferroelectric configurations can be written as

$$\frac{V_{dis}^{f(a)}}{k_B T} \propto \int_{L_a}^{L_a+L_c} dl_{1c} \int_0^{L_c} dl_{2c} \frac{\alpha_c^2}{[\{x \pm (l_{2c} \mp l_{1c}) \sin \theta\}^2 + (g + l_{2c} - l_{1c})^2 \cos^2 \theta]^3} \quad (2.25)$$

where α_c is the polarizability per unit length of the end chain of length L_c . L_a is the length of the aromatic core. As shown in Fig. 2.6, θ and x denote the tilt angle and horizontal separation of the molecules in the neighbouring layers respectively. We have assumed a small gap g between the smectic layers. The superscript "f(a)" denotes the interaction for ferroelectric (antiferroelectric) configurations with the upper sign corresponding to the ferroelectric configuration. The interaction energies calculated from Eq. 2.25 are shown in Fig. 2.7. The antiferroelectric configuration has a lower energy minimum compared to the ferroelectric configuration. However, it is clear from Fig. 2.7 that the energy difference between the two minima for one pair of molecules is also much less than $k_B T$. But, as the molecules are already ordered in each layer and they can move in unison, the relevant quantity is the energy difference between the two configurations per unit area which is of course quite substantial and far exceeds $k_B T$.

Further, this mechanism works for racemic mixtures as well as for achiral systems without any further assumptions. Also, as the angle made by the last C-C bond of the alkyl chain with the layer plane varies substantially between the odd and even members of a homologous series, the strong *odd-even* effect mentioned earlier can be understood from this mechanism (see Fig. 2.11).

However, the ferroelectric configuration allows a relatively free translational motion of the molecules between adjacent layers, and is favoured entropically at higher temperatures. Therefore the nearest neighbour *inter* layer interaction is expected to be temperature dependent and should change sign to favour ferroelectric configuration at higher temperatures and antiferroelectric configuration at lower temperatures. The simplest assumption is to take $J_1 = j(T_{AF} - T)$, where J_1 is defined in Eq. 2.30.

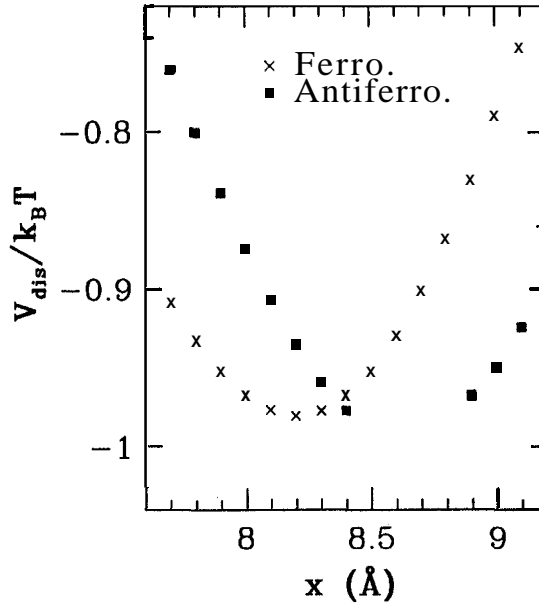


Fig. 2.7: The dispersion interaction V_{dis} between two molecules in adjacent layers as a function of the lateral separation x between them. The calculation has been done assuming $\theta = 0.5$ rad, $\alpha_c = 1.6$, $L_a = 10\text{\AA}$, $L_c = 8\text{\AA}$ and $g = 2\text{\AA}$.

Bruinsma *et al.* [21] also analyzed different types of interactions between the polarized smectic layers to account for the second and higher neighbour interactions. They have shown that the van der Waals and the elastic forces are weak compared to the forces which arise due to the correlated thermal fluctuation of polarization of the layers. By perturbative calculations, they found that the fluctuation force between the i -th and j -th layer is

$$V_{fluc}(i-j) \approx \Gamma \frac{S_i S_j}{|i-j|^2} \quad (2.26)$$

where Γ is given by

$$\Gamma = \frac{P_o^2}{4\epsilon d} \frac{k_B T}{\sqrt{K_{\parallel} K_{\perp}} \left(1 + \sqrt{\frac{K_{\parallel}}{K_{\perp}}}\right)^2} \quad (2.27)$$

where P_o is the polarization per unit area of the layers and K_{\parallel} , K_{\perp} are the appropriate anisotropic curvature elastic constants parallel and perpendicular to the layers. Since polarization $P_o \propto \theta$ and K_{\parallel} , K_{\perp} vary as θ^2 with the tilt angle θ , it is clear from Eq. 2.27 that Γ is independent of θ . This fact leads to the next nearest neighbour (NNN) J_3 term in Eq. 2.30.

Chiral intermolecular interactions can be quite complex. A well known and simple expression for the twist interaction between two rod like molecules i and j is [30]

$$H_{twist} = -\frac{1}{2} \sum_{ij} K(r_{ij}) (\hat{a}_i \cdot \hat{a}_j) (\hat{a}_i \times \hat{a}_j \cdot \hat{r}_{ij}), \quad (2.28)$$

where \hat{a}_i denotes the unit vector along the long axis of the i -th molecule and \vec{r}_{ij} is the intermolecular distance between the i -th and j -th molecules. After replacing \hat{a}_i by its average \hat{n}_i within the layer, this interaction in the tilted smectic phases takes the form [30]

$$f_{twist} = y_1 \sin 2\theta_i \sin 2\theta_j \sin(\phi_j - \phi_i) + y_2 \sin^2 \theta_i \sin^2 \theta_j \sin 2(\phi_j - \phi_i). \quad (2.29)$$

This form is consistent with the apolar nature of \hat{n} and gives rise to the Y_1 and Y_2 terms in Eq. 2.30 below. In analogy with the non-chiral NNN interaction, we introduced an NNN chiral Y_3 term in Eq. 2.30. This can be expected to be more important than a higher order ($\propto \theta^6$) first neighbour chiral interaction. As these chiral interactions can have many contributions we cannot guess the relative signs of the Y coefficients. For any given set, a reversal of the signs of all the coefficients would correspond to the opposite enantiomer.

2.4.2 The discrete model

In view of above observations we introduce a second neighbour antiferroelectric interaction which is independent of the tilt angle θ . Experimental observations clearly indicate that polarized layers are necessary for the occurrence of ferroelectric arid SmC_α^* phases and hence by implication, for the second neighbour antiferroelectric interaction. Using the order parameter defined in Eq. 2.2, we write the following phenomenological free energy per unit area for an N -layer system:

$$\begin{aligned} \mathcal{F}^{(N)} = & \sum_{i=1}^N \left[\frac{A'}{2} |\vec{\xi}_i|^2 + \frac{B}{4} |\vec{\xi}_i|^4 - \lambda \vec{\xi}_i \cdot \vec{P}_i + \frac{1}{2\chi} P_i^2 + J_1 (\vec{\xi}_i \cdot \vec{\xi}_{i+1}) \right. \\ & - \frac{J_2}{2} (\vec{\xi}_i \cdot \vec{\xi}_{i+1})^2 + J_3 (\hat{\xi}_i \cdot \hat{\xi}_{i+2}) + Y_1 (\vec{\xi}_i \times \vec{\xi}_{i+1}) \\ & \left. + Y_2 (\vec{\xi}_i \cdot \vec{\xi}_{i+1}) (\vec{\xi}_i \times \vec{\xi}_{i+1}) + Y_3 (\vec{\xi}_i \times \vec{\xi}_{i+2}) - \vec{E} \cdot \vec{P}_i \right], \quad (2.30) \end{aligned}$$

where A' and B are the usual Landau coefficients describing the second order SmA to SmC transition, with $A' = \alpha(T - T_{AC})$, T_{AC} being the SmA-SmC transition temperature, and arise from intra-layer interactions. $J_1 = j(T_{AF} - T)$, where T_{AF} is the temperature at which J_1 changes sign to favour ferroelectric interaction at higher temperatures.

Note that only upto quadratic terms in the secondary order parameter \vec{P} have been taken into account as the higher order terms are expected to be small. Also the terms with $(\vec{P}_{i+1} \cdot \vec{P}_i)$ are not taken into account as these are identically zero in the limit of infinite area as discussed in Sec. 2.4.1.

The Y coefficients correspond to chiral interactions between the layers. The term with coefficient λ is called *electroclinic* term in analogy with the piezoelectric term in solid state physics as it couples the polarization with the the tilt angle. This term as well as the Y -terms are allowed only in the chiral medium.

Minimization of Eq. 2.30 with respect to \vec{P}_i as in the continuous case yields

$$\vec{P}_i = \chi(\lambda \vec{\xi}_i - \vec{E}) \quad (2.31)$$

Elimination of \vec{P}_i from Eq. 2.30 using Eq. 2.31 gives

$$\begin{aligned} \mathcal{F}^{(N)} = \sum_{i=1}^N & \left[\frac{A}{2} |\vec{\xi}_i|^2 + \frac{B}{4} |\vec{\xi}_i|^4 + J_1 (\vec{\xi}_i \cdot \vec{\xi}_{i+1}) - \frac{J_2}{2} (\vec{\xi}_i \cdot \vec{\xi}_{i+1})^2 + J_3 (\hat{\xi}_i \cdot \hat{\xi}_{i+2}) \right. \\ & + Y_1 (\vec{\xi}_i \times \vec{\xi}_{i+1}) + Y_2 (\vec{\xi}_i \cdot \vec{\xi}_{i+1}) (\vec{\xi}_i \times \vec{\xi}_{i+1}) + Y_3 (\vec{\xi}_i \times \vec{\xi}_{i+2}) \\ & \left. - C (\vec{E} \cdot \vec{\xi}_i) \right] \end{aligned} \quad (2.32)$$

where $A = A' - \chi\lambda^2$ and $C = \lambda\chi$. To study the phase transition in the absence of electric field, we assume that the energy associated with the *soft* mode is much higher than that for *Goldstone* mode and hence the tilt angle of the layers is homogeneous *i.e.*, independent of i . X-ray studies on antiferroelectric liquid crystals appear to justify this assumption. With this assumption and using Eq. 2.2, the free energy Eq. 2.32 can be rewritten as

$$\begin{aligned} \mathcal{F}^{(N)} = \sum_{i=1}^N & \left[\frac{A}{2} \xi_o^2 + \frac{B}{4} \xi_o^4 + J_1 \xi_o^2 \cos(\phi_{i+1} - \phi_i) - \frac{J_2}{2} \xi_o^4 \cos^2(\phi_{i+1} - \phi_i) \right. \\ & + J_3 \cos(\phi_{i+2} - \phi_i) + Y_1 \xi_o^2 \sin(\phi_{i+1} - \phi_i) \\ & \left. + Y_2 \xi_o^4 \cos(\phi_{i+1} - \phi_i) \sin(\phi_{i+1} - \phi_i) + Y_3 \xi_o^2 \sin(\phi_{i+2} - \phi_i) \right], \end{aligned} \quad (2.33)$$

where $\xi_o = \sin 2\theta/2$ and θ is the tilt angle. To obtain the equilibrium configuration the free energy in Eq. 2.33 has to be numerically minimized as discussed below.

2.4.3 Calculations

The free energy given by Eq. 2.33 is minimized numerically using a multidimensional conjugate gradient method [41]. Starting from an initial guess this method in successive iterations minimizes the function along "non-interfering" or so called *conjugate* directions with the special property that minimization along one direction is not "spoiled" by subsequent minimization along another direction.

To make *conjugate* directions mathematically more explicit, first note that if we minimize a function along some direction \mathbf{u} , then the gradient of the function must be either zero or perpendicular to \mathbf{u} at the line minimum. Next consider some point \mathbf{P} as the origin of the coordinate system with coordinates \mathbf{x} . Then any function can be approximated by its Taylor series

$$\begin{aligned} f(\mathbf{x}) &= f(\mathbf{P}) + \sum_i \frac{\partial f}{\partial x_i} x_i + \frac{1}{2} \sum_{i,j} \frac{\partial^2 f}{\partial x_i \partial x_j} x_i x_j + \dots \\ &\approx c - \mathbf{b} \cdot \mathbf{x} + \frac{1}{2} \mathbf{x} \cdot \mathbf{A} \cdot \mathbf{x}, \end{aligned} \quad (2.34)$$

where

$$c \equiv f(\mathbf{P}) \quad \mathbf{b} \equiv -\nabla f|_{\mathbf{P}} \quad \mathbf{A}_{ij} \equiv \left. \frac{\partial^2 f}{\partial x_i \partial x_j} \right|_{\mathbf{P}} \quad (2.35)$$

The matrix \mathbf{A} whose components are the second partial derivatives of the function is called the *Hessian matrix* of the function at \mathbf{P} . In the approximation of Eq. 2.34, the gradient

of f is easily calculated as

$$\nabla f = \mathbf{A} \cdot \mathbf{x} - \mathbf{b} \quad (2.36)$$

Therefore the change in ∇f as we move along some direction is evidently

$$\delta(\nabla f) = \mathbf{A} \cdot (\delta\mathbf{x}). \quad (2.37)$$

Suppose that we have moved along some direction \mathbf{u} to a minimum and now propose to move along some new direction \mathbf{v} . The condition that the motion along \mathbf{v} not "spoil" our minimization along \mathbf{u} is just that the gradient stays perpendicular to \mathbf{u} , *i.e.*, that the change in gradient be perpendicular to \mathbf{u} . By Eq. 2.37 this is just

$$0 = \mathbf{u} \cdot \delta(\nabla f) = \mathbf{u} \cdot \mathbf{A} \cdot \mathbf{v} \quad (2.38)$$

When Eq. 2.38 holds for two vectors \mathbf{u} and \mathbf{v} , they are said to be *conjugate*. When the relation holds pairwise for all members of a set of vectors; they are said to be a conjugate set. If one does successive line minimization of a function along a conjugate set of directions, then there is no need to redo the minimization along any of those directions. Therefore, the algorithm reduces to finding the conjugate set and carry out successive line minimizations along those directions using an iterative procedure. We have used the Polak and Rebiere version of the algorithm (see [41] for detail) in our calculations.

Coming back to our problem, we assume that \mathbf{A} and \mathbf{B} coefficients in Eq. 2.33 are much larger than the \mathbf{J} and \mathbf{Y} coefficients, so that the magnitude ξ_o varies with temperature as $\xi_o^2 \approx \alpha(T_{AC} - T)/B$ below the SmA-SmC transition temperature. A typical set of parameters used in the calculations are as follows (in cgs units): $a = 0.088$, $\mathbf{B} = 13.8$, $j = 2.18 \times 10^{-4}$, $J_2 = 3.0 \times 10^{-4}$, $J_3 = 1.2 \times 10^{-5}$, $Y_1 = 8.0 \times 10^{-6}$, $Y_2 = 4.2 \times 10^{-4}$, $Y_3 = -1.47 \times 10^{-5}$, $T_{AC} = 379\text{K}$ and $T_{AF} = 367\text{K}$ (the last two values correspond to those of C8-tolane [33]).

In addition to the ferroelectric and antiferroelectric phases, this model gives rise to other stable *uniform* helical phases and a *nonuniformly* modulated phase. The profile of the \vec{c} -vector in different layers for these structures are shown in Fig. 2.8. The transition points between different phases are obtained by comparing the appropriate free energies.

2.4.4 Results and discussion

In the absence of chirality, and if $J_2 = 0$ it is easy to see from Eq. 2.33 that ferroelectric ($J_1 < 0$) and antiferroelectric ($J_1 > 0$) phases are stable when $|J_1|\xi_o^2 > 4J_3$. Otherwise there is a second order transition to an intermediate uniform helical structure with $64 = J_1\xi_o^2/4J_3$. Since there is no chirality the right handed and left handed structures are degenerate in this case.

The chiral terms in our model lift this degeneracy and drive these second order transitions from SmC_β^* to FI_H ($-\pi/2 < \delta\phi < 0$) and SmC_A^* to FI_L ($-\pi < \delta\phi < -\pi/2$), to first order. When $J_2 > 0$ and is sufficiently large, another ferrielectric phase FI_I develops. It is characterized by a nonuniform modulation with $\delta\phi_1$ between one pair of neighbours being different from $\delta\phi_2$ of an adjacent pair (see Fig. 2.8 and 2.9). In addition, when T approaches T_{AC} , $|J_1|\xi_o^2$ again becomes smaller than $4J_3$ and another ferriphase (SmC_α^*) is stabilized. Further, as first pointed out by Cepic *etal.* [40] close to T_{AC} , $\delta\phi$ in the

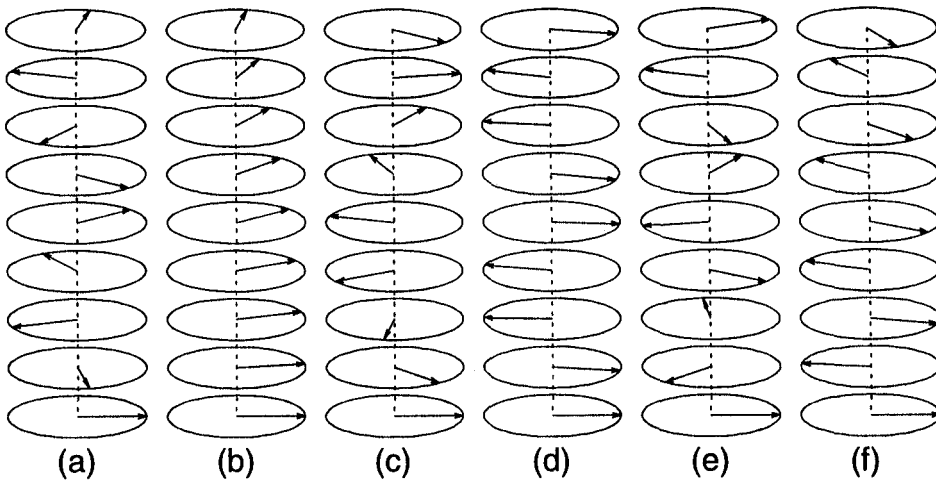


Fig. 2.8: Schematic representation of the structures of the various phases predicted by our model. The arrows indicate the c -vectors, the projections of the director on the smectic layers. In the representations of the helical structures in the (a) SmC_α^* (b) SmC_β^* (c) FI_H (d) FI_I (e) FI_L and (f) SmC_A^* phases, the differences in tilt angle in the different phases has been ignored.

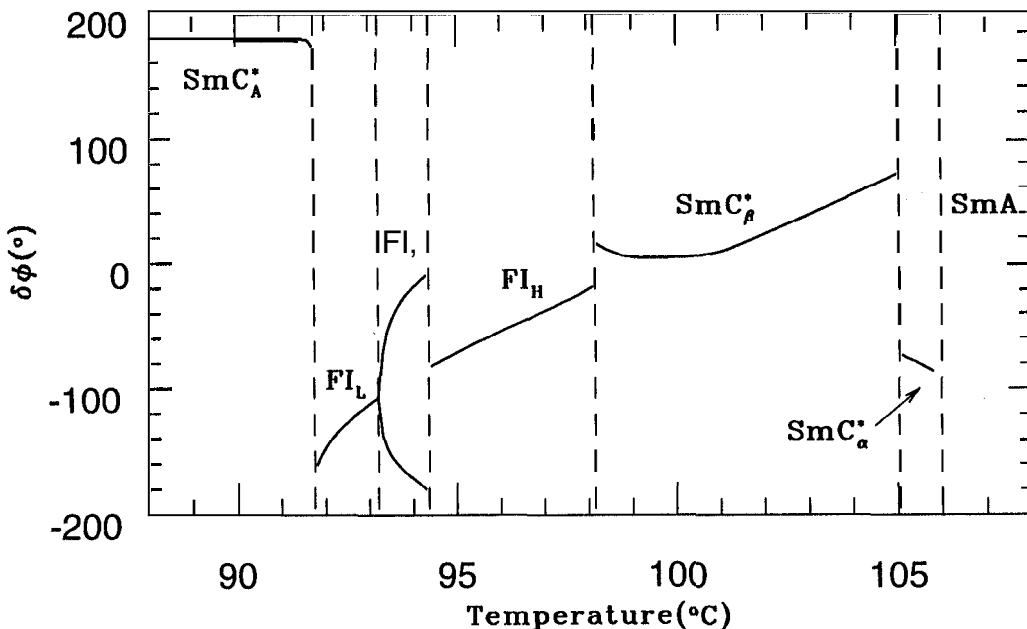


Fig. 2.9: Theoretical temperature variation of $\delta\phi$, the difference in azimuthal angles between successive layers for the parameters given in the text. $\delta\phi$ characterize the helical structure which is uniform in all the tilted phases except in the FI_I phase giving rise to the splitting of $\delta\phi$ in this phase.

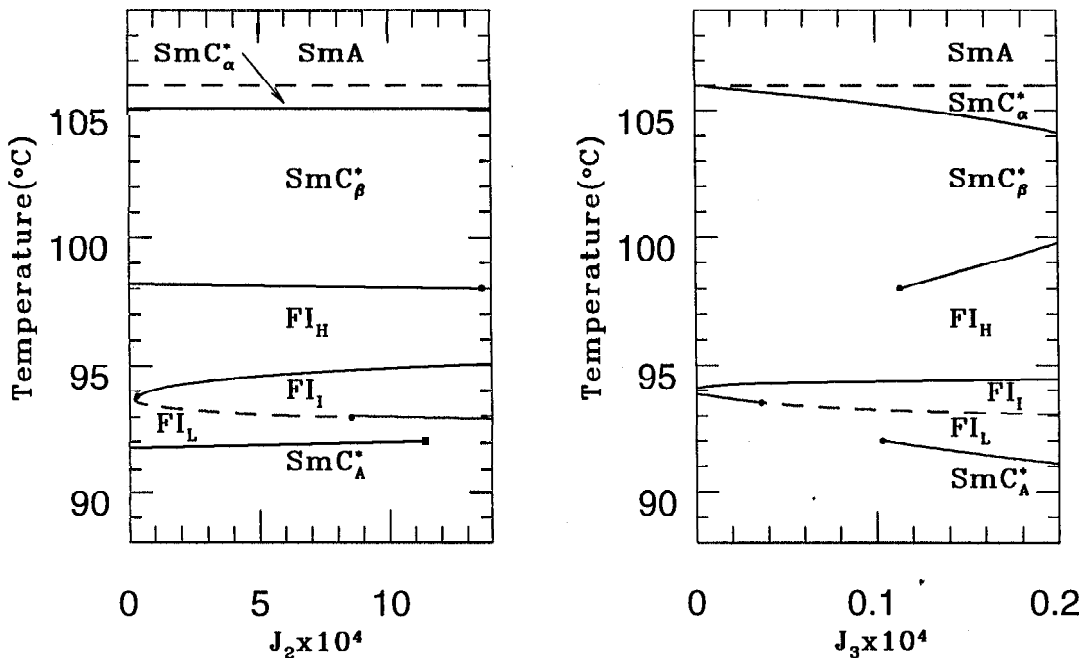


Fig. 2.10: (a) Temperature– J_2 phase diagram and (b) Temperature– J_3 phase diagram. Note the tricritical points in the phase boundary involving FI_I phase, and the critical points in the SmC^*_β - FI_H and FI_L - SmC^*_A phase boundaries. J_3 can be expected to decrease with chain length in a homologous series.

SmC^*_α phase approaches $\pi/2$ which explains the antiferroelectric character in the high temperature ranges of SmC^*_α phase seen experimentally [13].

Ignoring the tilt angle θ of the layers, the order parameter of the FI_I phase is related to the difference $(\delta\phi_1 - \delta\phi_2)$. In the other uniformly modulated phases, the order parameter is related to $\delta\phi (= \delta\phi_1 = \delta\phi_2)$ which changes in sign and magnitude across the different phase transitions. The global symmetry of all the uniform phases with a helical twist is the same and the phase transitions between them can only be 1st order in nature. These transitions involve jumps in $\delta\phi$, which do not cost too much energy. The entropy $S = -\partial F/\partial T$, and the heat of transition $T\Delta S$ between two phases is $(Tj\xi_0^2\Delta(\cos\delta\phi))$ which is typically ~ 1 joule/mole in broad agreement with the experimentally measured values [33].

The detailed phase diagrams when J_2 and J_3 are varied, keeping all the other parameters fixed, are shown in Fig. 2.10. In the J_2 -temperature phase diagram the phase boundary involving the FI_I phase has a parabolic shape which is characteristic of reentrant phenomenon. Also in part of the phase boundary (shown by dashed line) the transition between the nonuniform and uniform structures is second order in character. There are two tricritical points on this boundary beyond which the transition becomes first order in nature. Both SmC^*_β - FI_H and SmC^*_A - FI_L transition lines end in critical points as J_2 is increased as a consequence of the same global symmetry of the phases involved in these transitions. Depending on the value of J_2 we can have either one or three ferriphases

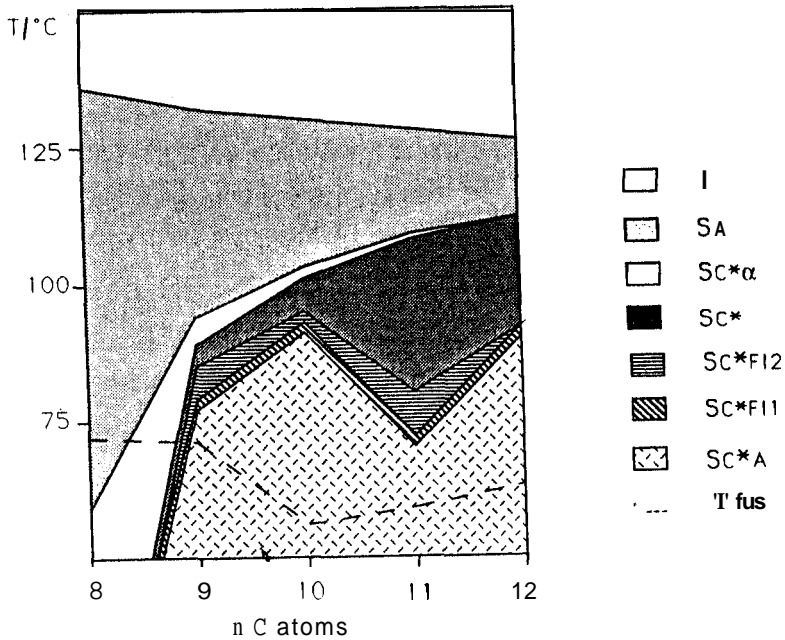


Fig. 2.11: Phase diagram as a function of the nonchiral end chain length in a homologous (nFF) series. J_3 can be expected to decrease with chain length in a homologue series. Note the odd-even effect on the transition temperatures involving the ferrielectric, SmC_β^* and SmC_A^* phases but not the transition temperature between the SmA and SmC_α^* phases. After Ref. [9].

(Fig. 2.10).

As J_3 arises from the fluctuations in the polarization of the layers, we can expect that it decreases for higher homologs in which the nonchiral end chain length is increased. As can be seen in Fig. 2.10, the ranges of both the SmC_α^* phase and the ferriphases are reduced as J_3 is decreased. This trend has been seen in many homologous series [9] as shown in Fig. 2.11. If an enantiomer of opposite chirality is added to an originally pure compound, the polarization of the layers is lowered. In this case both the J_3 and Y coefficients are reduced leading to a disappearance of the SmC_α^* and ferriphases as seen experimentally [6]. Both $\text{SmC}_\beta^*-\text{FI}_H$ and $\text{SmC}_A^*-\text{FI}_L$ transitions exhibit critical points as J_3 is lowered. In Fig. 2.10, the finite width of the FI_I phase even when $J_3 = 0$ arises from the second neighbour chiral interaction Y_3 .

2.5 Conclusions

The discrete chiral ANNNXY model developed by us for the antiferroelectric liquid crystals incorporating the correct symmetry of the tilted smectic layers accounts for the first time the entire sequence of phase transitions often seen in experiments. The very weak first order transitions between many of these phases arise from abrupt changes in $\delta\phi$ values, which are brought about by chiral interactions. In racemic mixtures the NNN J_3 -term

arising from the fluctuations of the polarizations as well as the chiral Y-terms will be zero and the ferroelectric phases will be absent as observed experimentally. Further, we will see in Chapter 3 and Chapter 4 that the various optical properties of the system in the presence and absence of a static field predicted by the model are in good agreement with the experimental observations.

The SmC_α^* phase has a very short pitch, and further, at higher temperatures, the $\delta\phi$ value approaches $\pi/2$, which will lead to antiferroelectric properties as seen in some experiments [13]. The $\delta\phi$ values vary rapidly with temperature in the ferri as well as SmC_α^* phases. Indeed there are strong visible fluctuations in these phases [10], which are also seen in ellipsometric measurements on relatively thick films [23] caused by the strong dependence of the pitch on temperature.

Chapter 3

Electric field induced structures in antiferroelectric liquid crystals

3.1 Introduction

As we have discussed in Chapter 1, in the ferroelectric SmC^* liquid crystals, consisting of chiral molecules, each layer is transversely polarized with the polarization \vec{P} along the direction of local C_2 symmetry axis ($A \times \hat{k}$). Moreover, chirality induces a spontaneous helical structure of A with its axis along the layer normal. Due to this helical structure, the in-plane polarization \vec{P} also has a helical arrangement with its axis along the layer normal and hence macroscopically $\langle \vec{P} \rangle = 0$. Therefore the term *helielectric* is more appropriate for the description of this structure. However, the uniform helical structure can be distorted by surface forces and/or by an external field and many theoretical and experimental studies address such problems.

Further, as we have discussed earlier, all the tilted phases exhibited by AFLC also have helicoidal structures in the bulk. Therefore, an interesting question is: what is the effect of a field which is applied perpendicular to the helical axis on these structures? Further, as mentioned earlier, the structures of the SmC_α^* and the ferroelectric phases have not been clearly established. A large number of experimental studies using static or dynamic electric field have been conducted on these systems. As mentioned in the previous chapter, these experimental observations are often qualitatively compared with the devil's staircase predicted by Ising models. However, there has been no detailed calculation based on any theoretical model on the effect of an external field on the structures exhibited by the antiferroelectric liquid crystals.

Motivated by this, we studied the effect of an in-plane static electric field on the structures predicted by our model. Our model has several parameters to account for the various sub-phases exhibited by antiferroelectric liquid crystals in the absence of electric field as described in Chapter 2. In the presence of an electric field, the free energy expression of our model may have many local minima depending on the parameters of the model and hence finding the global minimum is quite difficult. It is known that, even simple 1-dimensional models such as Frankel Kontorova or FK model and Chiral xy-model exhibit rich zero temperature (ground state) phase diagrams in the presence of field (for a

review see [39]). As already mentioned, for Ising spins arranged in a 1-d lattice, Bak *et al.* [38] have shown that if the interaction is long range and convex, the zero temperature structures follow a hierarchy as a function of field which is described as a *devil's staircase*. Chiral xy-models with convex [42] as well as nonconvex [43, 22] nearest neighbour (NN) interactions lead to other types of hierarchical structures as a function of field. They form a succession of *commensurate* structures for which the *average* angular separation between adjacent spins is a rational fraction of 2π .

In this chapter we will discuss in detail the influence of an external static electric field on the structures of the different phases exhibited by AFLC. In Sec. 3.2, we discuss the coupling of the transverse electric field with the orientational order in these phases. The field induced changes in the structure of ferroelectric SmC* liquid crystals which can be described by a continuous two component order parameter have been discussed by many authors [44]. As a theoretical background to our model, we will consider this case in Sec. 3.3. The chiral xy-model and ANNNI model are known to exhibit rich varieties of commensurate and incommensurate phases. In particular the structures predicted by the chiral xy-model and some of the basic definitions will be quite relevant to the discussion of our results. We briefly describe them in Sec. 3.4. In Sec. 3.5, we reconsider our discrete model described in Chapter 2 to include the effect of a static electric field applied in the plane of the smectic layers. The difficulties associated with the determination of the structures which gives the global minimum of the free energy and the numerical technique employed are described in Sec. 3.6. The field induced structures obtained at different temperatures are described in Sec. 3.7. In Sec. 3.8 and 3.9, we compute the experimentally measurable quantities *viz.* the so called apparent tilt angles θ_{app} in different phases and compare them with the available experimental results. Finally, we mention some of the main conclusions of this chapter in Sec. 3.10.

3.2 Electric field order parameter coupling

A static electric field \vec{E} imposed on a liquid crystalline sample has many physical effects, some of which are quite complex [27]. For simplicity we restrict our attention to the case of a perfectly insulating medium free of charge carriers. Even in this ideal situation, the coupling of an external electric field to the orientational order in chiral tilted smectic phases involves at least three different processes:

1. As the layers in the chiral tilted smectic phases are transversely polarized, there is a linear coupling of the form $-\vec{P} \cdot \vec{E}$ of the electric field \vec{E} with the transverse polarization \vec{P} of the layers.
2. The anisotropy of the dielectric constant has a quadratic coupling with the field. To be more explicit, neglecting the small biaxiality of the tilted layers, the static dielectric constant measured along (ϵ_{\parallel}) or perpendicular (ϵ_{\perp}) to the nematic director \hat{n} are different. Therefore, for a general direction of the electric field \vec{E} , the relation between the electric displacement \vec{D} and \vec{E} has the form

$$\vec{D} = \epsilon_{\perp} \vec{E} + (\epsilon_{\parallel} - \epsilon_{\perp})(\hat{n} \cdot \vec{E})\hat{n}. \quad (3.1)$$

The difference $\epsilon_a = \epsilon_{\parallel} - \epsilon_{\perp}$ may be positive or negative depending on the chemical structure of the constituent molecules. The contribution to the thermodynamic potential due to this anisotropy in dielectric constant is

$$-\frac{1}{4\pi} \int \vec{D} \cdot d\vec{E} = -\frac{\epsilon_{\perp}}{8\pi} E^2 - \frac{\epsilon_a}{8\pi} (\hat{n} \cdot \vec{E})^2. \quad (3.2)$$

The first term is independent of orientation. The second term favours parallel alignment (A collinear with \vec{E}) if $\epsilon_a > 0$, and perpendicular alignment if $\epsilon_a < 0$.

3. Certain distortions in the director A can induce a spontaneous electric polarization in the medium. This effect first predicted by Meyer [45] is called *flexoelectricity* in analogy with piezoelectricity in solid state physics. The coupling of the electric field with the flexoelectric polarization may also induce distortions in the bulk.

In our theoretical calculations, we have neglected the dielectric coupling as a first approximation. This simplification is often employed in the theory of ferroelectric liquid crystals for usual fields used in experiments, as for low fields this quadratic coupling is relatively weak compared to the linear ($-\vec{P} \cdot \vec{E}$) term. However, some theoretical calculations have also been made on the SmC^* phase including this dielectric coupling. In our discrete model of AFLC, we also ignore the flexoelectric coupling. In ferroelectric liquid crystals, this coupling is known to be usually weaker compared to the other two couplings mentioned above.

3.3 SmC^* under a transverse electric field

In the bulk SmC^* phase (as described in Chapter 1) each layer is uniformly polarized in the plane of the layer and the transverse polarization has uniform helical arrangement along the layer normal (Fig. 3.1a). Now if an electric field \vec{E} is applied perpendicular to the axis of the helix, then, at arbitrarily small fields, the only possibility is that those parts of the helix where \vec{P} is locally parallel to \vec{E} expand. Because of the periodicity of \vec{P} , this means that the unfavourable regions where \vec{P} is antiparallel to \vec{E} shrink. In this scenario, the effect of the field is to produce a *soliton lattice structure* (SLS) which consists of domains in which \vec{P} is mostly parallel to \vec{E} . These domains are separated by a periodic array of walls with a spacing given by the pitch as sketched in Fig. 3.1b. Within a wall \vec{P} rotates through 2π to match the orientations of the domains on either side of it and is referred to as a 2π -wall. As the field is increased, the width of the domains increases at the expense of the width of the walls. If the interaction between the solitons are taken into account theoretically the soliton lattice spacing increases with field. However, as pointed out by Cladis [44] in the layered SmC^* phase this is unlikely to happen. Beyond a critical field, there is a transition to the fully unwound SmC^* structure as shown in Fig. 3.1c.

To describe this structure mathematically, we assume that the pitch of the helix is much longer than the layer spacing. Then the order parameter in Eq. 2.2 in the continuum limit becomes

$$\vec{\xi}(z) = (n_z n_y, -n_z n_x) = \frac{\sin 2\theta}{2} (\sin \phi, -\cos \phi), \quad (3.3)$$

where we have assumed that the smectic layers are flat (parallel to the xy-plane) with the layer normal along the z-axis and that the modulation of $\vec{\xi}$ is only along that axis.

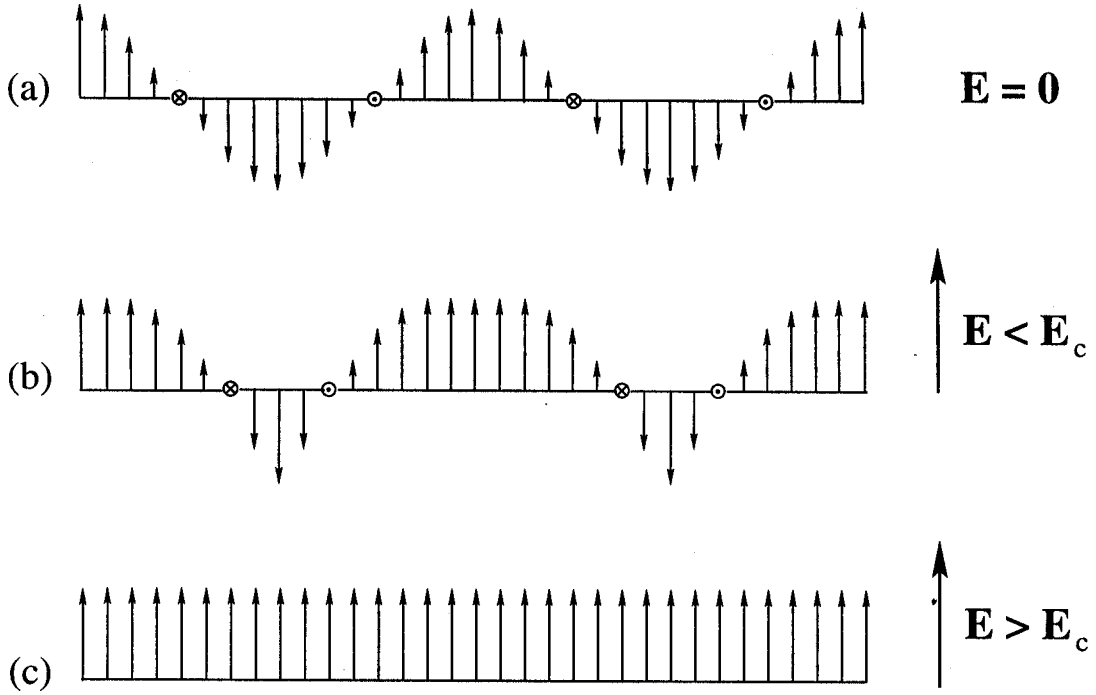


Fig. 3.1: Schematic representations of the helix unwinding in the presence of electric field applied perpendicular to the helix axis.

Using the above order parameter and the in-plane polarization \vec{P} as the secondary order parameter, the free energy per unit area in the presence of a static electric field \vec{E} applied in the plane of the layers can be written as

$$\begin{aligned}
 F = \int & \left[\frac{a}{2} \xi^2 + \frac{B}{4} \xi^4 - \lambda \vec{\xi} \cdot \vec{P} + \frac{P^2}{2\chi} + \frac{K}{2} \left(\frac{d\vec{\xi}}{dz} \right)^2 \right. \\
 & \left. + \delta \left(\xi_x \frac{d\xi_y}{dz} - \xi_y \frac{d\xi_x}{dz} \right) - \mu_f \left(P_x \frac{d\xi_y}{dz} - P_y \frac{d\xi_x}{dz} \right) - \vec{P} \cdot \vec{E} \right] dz \quad (3.4)
 \end{aligned}$$

where the sixth term is the Lifshitz invariant, A , μ_f are electroclinic and flexoelectric coefficients respectively. The last term is the linear coupling of transverse polarization \vec{P} of the layers with the electric field \vec{E} as mentioned earlier. We have neglected the contribution due to the dielectric anisotropy.

Eliminating \vec{P} after minimizing with respect to it, the free energy density F (Eq. 3.4) can be reexpressed in terms of the tilt angle θ and azimuthal angle ϕ as

$$\begin{aligned}
 F = \int & \left[\frac{a}{2} \theta^2 + \frac{B}{4} \theta^4 + \frac{K}{2} \left(\frac{d\theta}{dz} \right)^2 + \frac{K}{2} \theta^2 \left(\frac{d\phi}{dz} - q_0 \right)^2 \right. \\
 & \left. - \chi \lambda E \theta \sin \phi \right] dz \quad (3.5)
 \end{aligned}$$

where the electric field is assumed to be applied along the x direction, $q_0 = -(S + \chi \lambda \mu_f) / (K - \chi \mu_f^2)$ and the approximation $\sin \theta \approx \theta$ is utilized. Further, dividing F by

SECTION 3.3

B and making the transformations

$$\begin{aligned} u &= q_0 z \\ \rho &= q_0 \sqrt{\frac{K}{B}} \theta \\ \tilde{E} &= \frac{\chi \lambda}{q_0 \sqrt{BK}} E, \end{aligned} \quad (3.6)$$

the free energy F in Eq. 3.5 can be rewritten as

$$F = F_0 \int \left[\frac{A}{2} \rho^2 + \frac{1}{4} \rho^4 + \frac{1}{2} \left(\frac{d\rho}{du} \right)^2 + \frac{1}{2} \rho^2 \left(\frac{d\phi}{du} - 1 \right)^2 - \tilde{E} \rho \sin \phi \right] du \quad (3.7)$$

in which $A = a/B = \alpha(T - T_0)$ is temperature dependent; a and T_0 are constants.

Let us first consider the case of p being constant ($= \rho_0$) determined by the relation $\rho_0^2 + A = 0$ for temperatures below T_0 neglecting the "weak" modulation terms. The ϕ -dependent part of the free energy then becomes

$$F = \int \left[\frac{\rho_0^2}{2} \left(\frac{d\phi}{du} - 1 \right)^2 - \tilde{E} \rho_0 \sin \phi \right] du \quad (3.8)$$

and the Euler-Lagrange equation corresponding to the variation of ϕ is

$$\rho_0^2 \frac{d^2 \phi}{du^2} - \tilde{E} \rho_0 \cos \phi = 0. \quad (3.9)$$

Eq. 3.9 is the well studied static sine-Gordon equation.

The 1-soliton solution of Eq. 3.9 with the boundary conditions $\phi = 0$ as $u \rightarrow -\infty$, and $\phi = 2\pi$ as $u \rightarrow \infty$ can be written as

$$\phi = 4 \tan^{-1} \{ \exp[(u - u_0)/\rho_0] \}. \quad (3.10)$$

The profile of this 1-soliton solution is shown in Fig. 3.2. A periodic solution of Eq. 3.9 is obtained by quadrature as [44]

$$\phi = -2 \sin^{-1} \{ \text{sn}[(u - u_0)/\rho_0 k, k] \} - \frac{\pi}{2}, \quad (3.11)$$

where $\text{sn}(x, k)$ is Jacobi's sn function and k (≤ 1) the modulus coming from the integration constant. This solution with $k < 1$ is called the *soliton lattice* and it reduces to Eq. 3.10 in the limit $k \rightarrow 1$.

For the general case, taking into consideration the variation of ρ , the stationary condition for the free energy functional F (Eq. 3.7) leads to the Euler-Lagrange equations

$$A\rho + \rho^3 - \frac{d^2 \rho}{du^2} + \rho \left(\frac{d\phi}{du} - 1 \right)^2 - \tilde{E} \sin \phi = 0, \quad (3.12)$$

$$\rho^2 \frac{d^2 \phi}{du^2} + 2\rho \frac{d\rho}{du} \left(\frac{d\phi}{du} - 1 \right) - \tilde{E} \rho \cos \phi = 0. \quad (3.13)$$

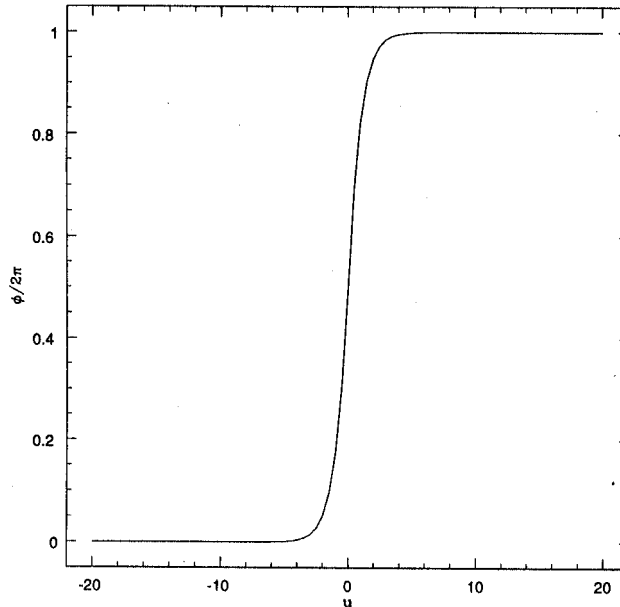


Fig. 3.2: The 1-soliton solution with $\rho_0 = 0.8$.

A first integral of Eq. 3.12 and 3.13 can be written as

$$\frac{1}{2} \left(\frac{d\rho}{du} \right)^2 + \frac{\rho^2}{2} \left(\frac{d\phi}{du} \right)^2 = \frac{1}{2}(A+1)\rho^2 + \frac{1}{4}\rho^4 - \tilde{E}\rho \sin \phi + C, \quad (3.14)$$

where C is an integration constant. However, up to now no analytic solutions of Eq. 3.12 and 3.13 have been found. The ρ and ϕ profiles as functions of u obtained numerically by Yamashita *et al.* [44] are shown in Fig. 3.3. As a uniform solution to Eq. 3.12 and Eq. 3.13 corresponding to the unwound ferroelectric phase, we obtain $\phi = (2m + 1/2)\pi$ with integer m and $\rho = \rho_0$, determined from

$$(A+1)\rho_0 + \rho_0^3 - \tilde{E} = 0. \quad (3.15)$$

3.4 Commensurate and incommensurate structures

A wide variety of complicated spatially modulated structures have been observed in numerous condensed matter systems. Such structures arise not only in non equilibrium situations, for instance as a response to a change in an external parameter or by sustaining boundary conditions that prevent thermalization of the system, but also occur in thermal equilibrium state of an ensemble of particles. The modulation may be in the positions of the particles or in some local property such as the magnetization, charge density, electric polarization or chemical composition. It is often periodic, and the periodicity may be *commensurate* or *incommensurate* with that of the reference lattice.

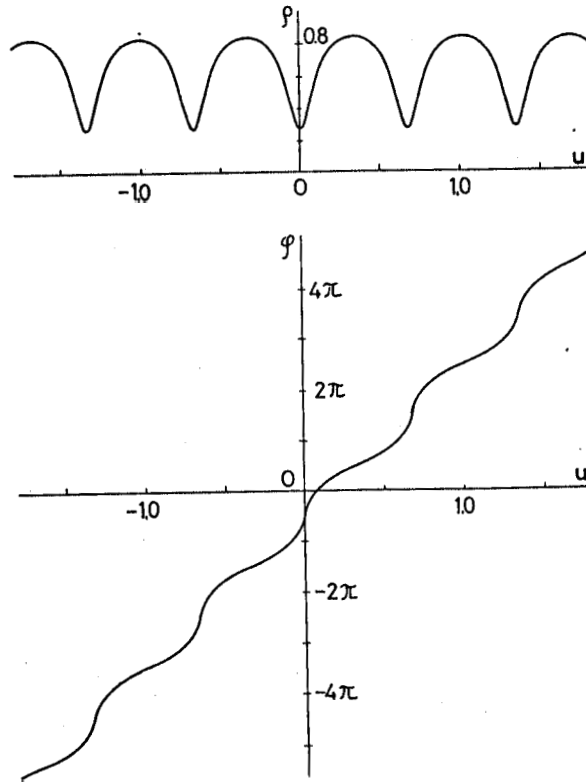


Fig. 3.3: Soliton lattice solutions for ρ and ϕ numerically obtained by Yamashita. After Ref. [44].

On the theoretical side, one possible origin for such commensurate or incommensurate structures is the competition between, at least, two interactions that favour different commensurate structures. Several phenomenological descriptions of spatially modulated patterns have been used to discuss general features and also to interpret specific experiments. In particular, the models such as Frankel-Kontorova or FK model, Axial Next Nearest Neighbour Ising or ANNNI model and Chiral xy-model are known to exhibit complex phase diagrams comprising of simple commensurate, long period commensurate and incommensurate phases.

In our model, the configuration of each tilted smectic layer is described by a 2-d axial vector and these layers are coupled through both chiral and nonchiral interactions. Therefore, an analogy with the chiral xy model can be invoked. In fact a theoretical study [22] of chiral xy model with nearest neighbour (NN) interactions has shown that though the model is quite trivial in absence of a field, it exhibits a rich ground state phase diagram for nonzero fields. In general the stable phases can be commensurate or incommensurate and can follow a devil's staircase with increasing field as described below.

3.4.1 Basic definitions

Let us consider the physical properties $A_i (i = 1, 2, \dots)$ of a material that displays periodic spatial modulations characterized by wave vectors \vec{q}_i . The modulations of the two quantities A_1 and A_2 are said to be commensurate (C) with each other when

$$r_\alpha = \frac{q_{\alpha 2}}{q_{\alpha 1}} \quad (\alpha = x, y, z) \quad (3.16)$$

are rational numbers for all Cartesian coordinates. If at least one of the three ratios is an irrational number then A_1 and A_2 are said to form spatial structures that are incommensurate (IC) with each other.

For instance, A_1 may describe the position of the atoms in a lattice, the periodicity being characterized by the reciprocal lattice vector and A_2 the magnetic or electric moments or spins carried by the atoms. Trivial examples of commensurate structures are the ferromagnetic ($r_x = 0$) and antiferromagnetic ($r_x = 1/2$), states. In a layered helical structure the commensurability ratios are given by

$$r_x = r_y = 0, \quad r_z = \phi/360, \quad (3.17)$$

where ϕ is the angle between the orientations of the magnetic moments in the adjacent xy layers. If r_z is irrational, i.e in the incommensurate case, the repeat distance for a given orientation is infinite. Obviously, the repeat distance is two lattice constants in the antiferromagnetic structure, and one in the ferromagnetic case.

In general, the commensurability measured by r_α , for a specific material will depend on external parameters, such as temperature or electric and magnetic fields. Various scenarios are possible. For instance, r_α may vary smoothly with the external parameter p , as depicted in Fig. 3.4a. This behaviour implies that rational values of r_α occur only with measure zero in each finite range of variation in p , while the irrational values take the entire measure of that range. The material is then said to display an incommensurate phase through the range of variation. In other circumstances $r_\alpha(p)$ may lock in at a finite

SECTION 3.4

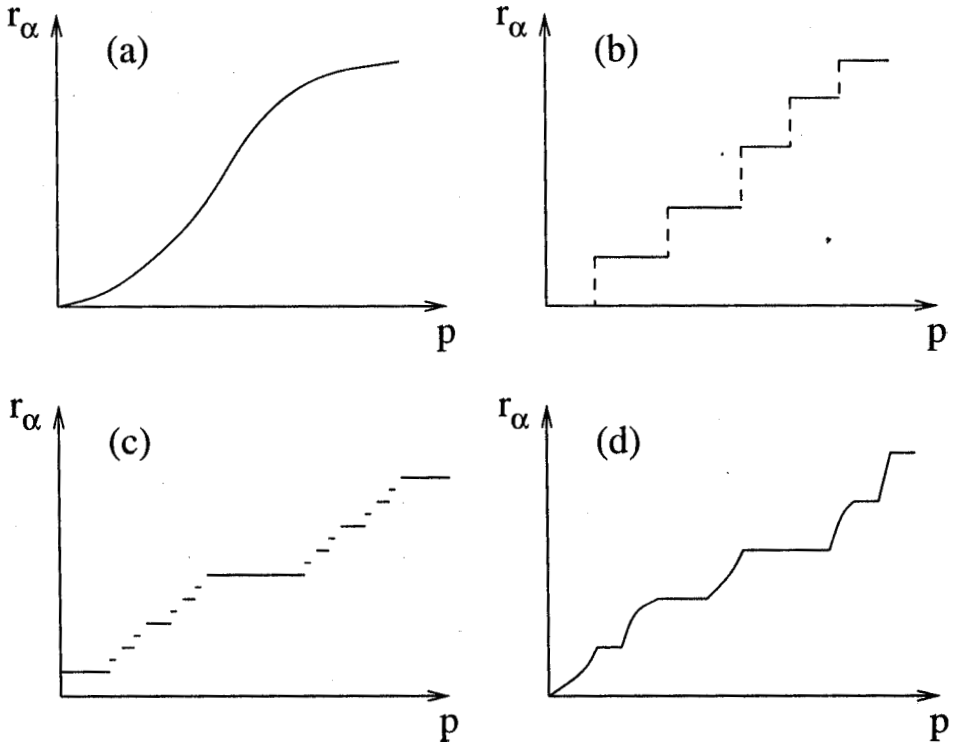


Fig. 3.4: Schematic representations of four possible scenarios of variation of the commensurability r_α with the parameter p : (a) smooth analytic variation in the incommensurate phase, (b) harmless staircase, (c) complete devil's staircase and (d) incomplete devil's staircase.

number of rational values (Fig. 3.4b). Such a sequence of commensurate phases, separated by first order transitions, has been called a *harmless staircase* [46]. By contrast, in a *devil's staircase* $r_\alpha(p)$ has infinitely many plateaus, with quasi continuous transitions on going from one structure to another. The devil's staircase is said to be *complete* if the sum of the plateau widths is identical with the range of variation in p ; usually (but not necessarily), the steps occur at each rational value of r . A complete devil's staircase is sketched in Fig. 3.4c. If the sum is smaller than the interval, *i.e.*, if r , changes smoothly (with a nonzero derivative) over some parts of the interval, then the devil's staircase is called an *incomplete* one (Fig. 3.4d).

3.4.2 1-d Chiral xy model

Consider a model consisting of a system of 2-d classical spins arranged in a 1-d lattice. The spins interact through nearest neighbour chiral interactions and are subjected to an external field. The Hamiltonian of the system is given by

$$H(\{\theta_n\}) = \sum_n [W(\theta_n - \theta_{n-1}) + V(\theta_n)], \quad (3.18)$$

where

$$W(x) = 1 - \cos(x - A) \quad (3.19)$$

and

$$V(x) = E(1 - \cos px). \quad (3.20)$$

Here θ_n is the angle between the spin vector at the n th site and the applied field, A is the chirality parameter and E is the magnitude of the field. The problem is to study the ground state configurations of the spins at absolute zero of temperature.

Quite a few models similar to the one above have been studied in the past in connection with systems exhibiting modulated structures. Perhaps the most extensively studied model of this kind is the Frankel Kontorova (FK) model. In FK model the inter spin potential W is strictly *convex* with the form $W(x) = \frac{1}{2}(x - \Delta)^2$ and $p = 1$ in Eq. 3.20. Aubry *et al.* [42] found many rigorous results for a class of systems described by Eq. 3.18 with W being strictly *convex*.

The 1-d chiral xy model with *nonconvex* W given by Eq. 3.19 but with $p = 2$ in Eq. 3.20 has been studied by Banerjee *et al.* [43]. They found a field induced devil's staircase in this model. Yokoi *et al.* [22] also studied the 1-d chiral xy model with $p = 1$ in Eq. 3.20 in great detail. They used an improved numerical technique *viz.* the so called *effective potential method* developed by Chou *et al.* [47] to construct the field versus A phase diagram as shown in Fig. 3.5. Different commensurate phases are designated by the following notation: For a ground state configuration $\{\theta_n\}$, the average spin rotation in a period is defined as

$$q \equiv 2\pi\bar{q} = \langle \theta_n - \theta_{n-1} \rangle. \quad (3.21)$$

with the convention that $0 \leq \theta_n - \theta_{n-1} < 2\pi$. For a commensurate phase \bar{q} is taken to be a fraction P/Q with Q the period of the commensurate configuration and P the number of complete turns of 2π over a period. Hence the $\frac{1}{2}$ phase, which has a period 2 structure and an angular advance of 2π in each period should be distinguished from the $\frac{2}{4}$ phase, which has a period 4 structure and an angular advance of 4π in each period.

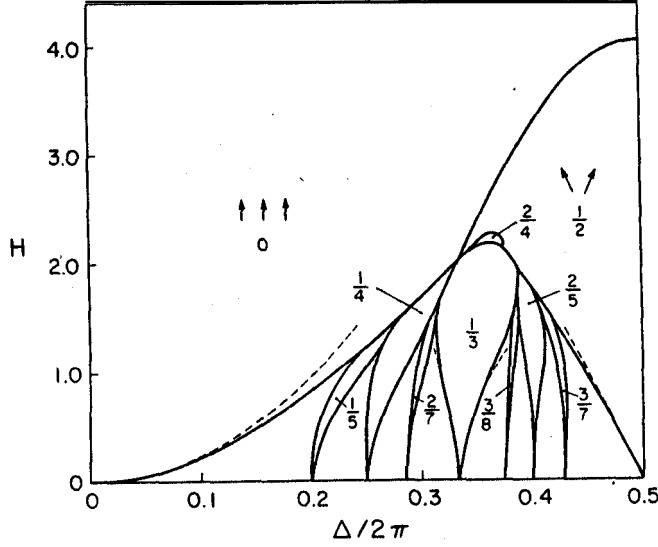


Fig. 3.5: The numerically obtained phase diagram of the 1-d chiral xy-model in the presence of a field. After Ref. [22].

With this background, we will now analyze the influence of an externally applied static electric field on the structures of the different phases exhibited by AFLC. We will show that the field induces new commensurate and incommensurate structures in different phases and the apparent tilt angle corresponding to these field distorted structures agree well with the experimental observations.

3.5 AFLC under transverse electric field

In Chapter 2 we have considered only the zero field limit of our model to account for the different phases exhibited by AFLC. In order to study the influence of an external static electric field \vec{E} applied in the plane of the smectic layers, the free energy density in Eq. 2.32 now has to be minimized including the field term. Let us rewrite Eq. 2.32 for this purpose as

$$\begin{aligned}
 \mathcal{F}^{(N)} = & \sum_{i=1}^N \left[\frac{A}{2} |\vec{\xi}_i|^2 + \frac{B}{4} |\vec{\xi}_i|^4 + J_1 (\vec{\xi}_i \cdot \vec{\xi}_{i+1}) - \frac{J_2}{2} (\vec{\xi}_i \cdot \vec{\xi}_{i+1})^2 + J_3 (\hat{\xi}_i \cdot \hat{\xi}_{i+2}) \right. \\
 & + Y_1 (\vec{\xi}_i \times \vec{\xi}_{i+1}) + Y_2 (\vec{\xi}_i \cdot \vec{\xi}_{i+1}) (\vec{\xi}_i \times \vec{\xi}_{i+1}) + Y_3 (\vec{\xi}_i \times \vec{\xi}_{i+2}) \\
 & \left. - \chi \lambda (\vec{E} \cdot \vec{\xi}_i) \right] \quad (3.22)
 \end{aligned}$$

where A and B are the usual Landau coefficients describing the second order SmA to SmC transition, with $A = a(T - T_{AC})$. The coefficient $J_1 = j(T_{AF} - T)$ changes sign at T_{AF} , favouring antiferroelectric NN order below T_{AF} . The terms with Y -coefficients are the chiral interactions. Note that the NNN J_3 interaction is associated with the unit vector $\hat{\xi}$ for reasons already discussed in Chapter 2. The last term in Eq. 3.22 arises from the

linear coupling of electric field $\vec{I}^?$ with the polarization \vec{P}_i of the layers and the relation $\vec{P}_i = \chi(\lambda\xi_i - \vec{I}^?)$ from Eq. 2.31. Again as in the case of the SmC* phase, we have neglected the coupling of \vec{E} with the dielectric anisotropy. We have also neglected the flexoelectric coupling of the field as mentioned earlier.

It should be mentioned here that our model differs from the 1-d chiral xy model described above in at least two aspects. Unlike the 1-d chiral xy model in which the spins are assumed to be of unit magnitude, in our model, the tilt angle θ of the director \hat{n} within the layer may change under the application of the field. Hence the magnitudes as well as the orientations of the order parameters are variable in this case. In addition, the magnitude of $|\xi|$ itself depends on the temperature as discussed in chapter 2. Secondly, our model involves in addition to the nearest neighbour interactions, the next nearest neighbour interactions. These two additional features of our model make the numerical calculations very difficult as described below.

3.6 Computational methods and difficulties

In spite of the apparent simplicity of even the simpler 1-d chiral xy-model discussed in Sec. 3.4.2, finding the ground state configurations of this type of a model is a formidable task. One approach to find the stable configuration, starts with the equilibrium equations obtained by equating the first partial derivatives of the free energy to zero and identifying the problem with some dynamical map. In some cases this dynamical map is area preserving or the so called *standard* map. There are many powerful theorems of standard maps already known in the literature which can then be directly applied to the problem. However, the major drawbacks of this approach are: (i) the equilibrium equations hold good for stable, meta stable as well as unstable solutions. Therefore further analysis is required for finding the solution corresponding to the global minimum. (ii) The dynamic map obtained from the equilibrium equations are single valued only when the inter spin interaction is strictly *convex*.

To overcome these difficulties Chou *et al.* [47] developed a method called the effective potential method. This method finds the global minimum solution and works for both convex as well as non convex interactions (see Sec. 5.3.1). However, the method is developed taking into account only the nearest neighbour interactions. We have not found in the literature a generalization of the method taking into account the next nearest or higher neighbour interactions. We found that a straightforward generalization including the next nearest neighbour interactions is computationally formidable. Further, the method assumes a constant magnitude of the spins which is not valid in our problem.

In view of these difficulties, we took a simpler approach to the problem. In our numerical algorithm, we first prepare the approximate initial guess solution corresponding to a given commensurability using a program. We then feed this approximate guess to a minimization routine to find the actual solution corresponding to that commensurability which minimizes the free energy given by Eq. 3.22. We have used the multidimensional conjugate gradient method in our minimization routine as described in Chapter 2. Our minimization routine also produces soliton lattice structures when the zero field structure was allowed to evolve under the field. Finally the ground state energies of all the low-order commensurate structures as well as soliton lattice solutions are compared to get the global

SECTION 3.7

Parameters	Values
α	0.088
T_{AC}	106.0°C
B	13.8
j	2.178×10^{-4}
T_{AF}	94.0°C
J_2	8.0×10^{-4}
J_3	1.2×10^{-5}
Y_1	8.0×10^{-6}
Y_2	4.18×10^{-4}
Y_3	-1.446×10^{-5}

Table 3.1: A typical set of values (in cgs units) of the parameters used in the calculation

minimum. Though our method is not exhaustive, it already gives rise to Structures whose optical properties agree quite well with experimental observations. A typical parameter set used in the calculation is shown in table 3.1. The number of layers N used in the calculations varies from 400 to 900.

3.7 Field induced structures in AFLC

3.7.1 Structures in antiferroelectric phase

The SmC_A^* phase has a uniform helical structure in the absence of a field. The azimuthal angle ϕ_l in the l th layer varies with l as $\phi_l = l(\pi - \alpha)$ where α ($\approx 2^\circ$) is a small angle. At low fields applied along the y-axis, this uniform helical structure gets distorted in such a way that the NN pairs whose net polarizations \vec{P}_f have favourable orientations with respect to the field grow at the expense of those with unfavourable orientations and a soliton lattice structure (SLS) is stabilized. Thus the SLS consists of domains with \vec{P}_f mostly parallel to \vec{E} and these domains are separated by periodic array of walls where the \vec{P}_f rotates by 2π as shown in Fig. 3.6. The corresponding variation of the tilt angle θ_i is shown in Fig. 3.7. As the field is increased, the widths of the domains increase at the expense of the widths of the walls and the difference in azimuthal angle between successive layers also decreases. Beyond a threshold field E_{c1} , this goes over to the commensurate structure of commensurability $1/2$. In this $1/2$ phase, the layers are uniformly tilted and the orientation of successive layers is ϕ and $-\phi$ respectively with respect to the x-axis as shown in (Fig. 3.8a). As the field is increased further, ϕ decreases and beyond a second threshold field E_{c2} , there is a transition to the fully unwound **ferro** phase of commensurability 0.

To estimate E_{c2} , notice that the solution corresponding to the $1/2$ commensurate structure is of the form

$$\phi_i = (-1)^i \phi \quad i = 1 \dots N, \quad (3.23)$$

where ϕ_i denotes the angle made by $\vec{\xi}_i$ with respect to \vec{E} . Neglecting the variation of the

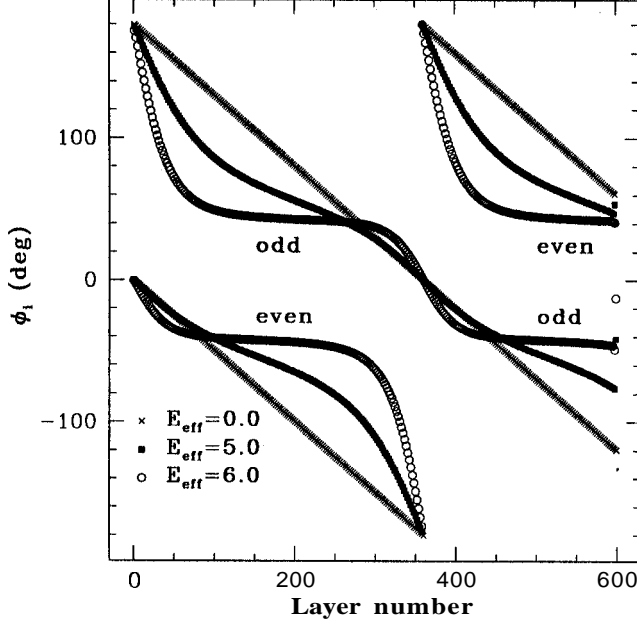


Fig. 3.6: The ϕ profile as a function of layer number in the antiferroelectric soliton solution which has two branches corresponding to the odd and even numbered layers. Field is assumed to be applied along the y-axis.

tilt angle θ with field, the free energy per layer (in the limit of infinite N) can be obtained by substituting ϕ_i from Eq. 3.23 as

$$f = J_1 \xi_o^2 \cos 2\phi - J_2 \xi_o^4 \cos^2 2\phi + J_3 - E \xi_o \cos \phi. \quad (3.24)$$

Just above E_{c2} , the unwound ferroelectric phase corresponding to $\phi = 0$ is stable whereas below E_{c2} the $1/2$ phase with nonzero value of ϕ is stable. Since close to the critical field E_{c2} , ϕ is small, we can expand the free energy given by Eq. 3.24 in powers of ϕ to determine the critical field as well as the order of the transition. Expanding f in Eq. 3.24 in a Taylor series about $\phi = 0$ and retaining only upto 6th order terms, the excess free energy with respect to the unwound ferroelectric phase (after dividing by the constant factor ξ_o) can be written as

$$f = \frac{A}{2} \phi^2 + \frac{B}{4} \phi^4 + \frac{\tilde{C}}{6} \phi^6, \quad (3.25)$$

where

$$\begin{aligned} \tilde{A} &= E - 4\xi_o(J_1 - J_2\xi_o^2), \\ \tilde{B} &= (16J_1\xi_o - 64J_2\xi_o^2 - E)/6, \\ \tilde{C} &= (E - 64J_1\xi_o + 1024J_2\xi_o^3)/120. \end{aligned} \quad (3.26)$$

It is now easy to see from Eq. 3.25 that the unwound ferroelectric phase is stable when $A > 0$ whereas the $1/2$ structure is stable when $A < 0$. Therefore, E_{c2} can be obtained by

SECTION 3.7

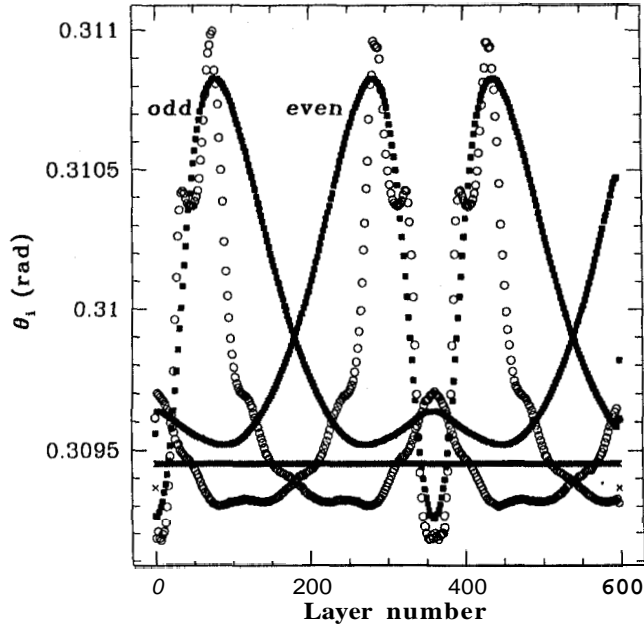


Fig. 3.7: The θ profile as a function of layer number in the antiferroelectric soliton solution. Note that $|\vec{\xi}| = \sin 2\theta/2 \sim \theta$ and the maximum change in θ is ~ 0.002 radians. The fields corresponding to the symbols are same as in Fig. 3.6.

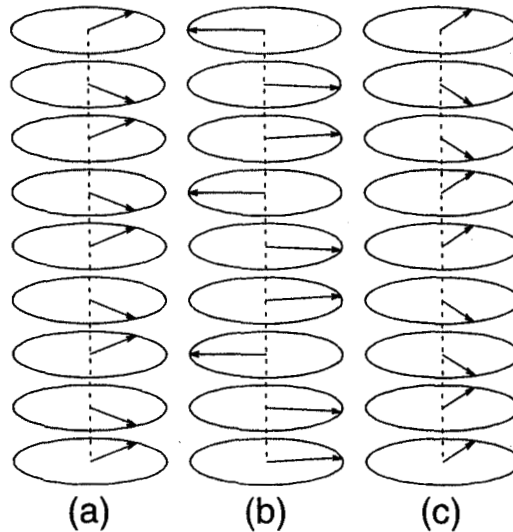


Fig. 3.8: The orientation of \hat{c} in a few layers for field induced *commensurate* structures (a) $1/2$ structure of SmC_A^* phase for $E_{eff} = 5.0$ (b) the $2/3$ structure of Fl_L phase for $E_{eff} = 2.0$ and (c) the $2/4$ structure in SmC_α^* phase for $E_{eff} = 1.6$. $\vec{E}_{eff} = 10^4 C \vec{E}$ is perpendicular to the plane of the figure (y-axis). The magnitude of \vec{c} reduces sharply in SmC_α^* phase compared to that in the other phases. Note that the polarization \vec{P} is perpendicular to \hat{c} in the layers.

equating \tilde{A} to zero and we get

$$E_{c2} = 4\xi_o(J_1 - J_2\xi_o^2). \quad (3.27)$$

Further the coefficient \tilde{B} is positive when $5J_2\xi_o^2 < J_1$ and if B is negative, the coefficient of the 6th order term \tilde{C} is positive. Therefore the transition is second order in nature when $5J_2\xi_o^2 < J_1$ and becomes first order when $5J_2\xi_o^2 > J_1$. The point $5J_2\xi_o^2 = J_1$ where $B = 0$ corresponds to a tricritical point (TCP).

3.7.2 Structures in ferrielectric phases

In the ferrielectric FI_L and FI_I phases the soliton lattice structures (SLS) are favoured at low fields. As the field is increased, the SLS structure goes over to the $2/3$ commensurate structure (Fig. 3.8b) at a threshold field. The $2/3$ commensurate structure remains stable over a fairly wide range of fields. As the field is increased further, the soliton structure *reenters* and remains stable until the fully unwound ferroelectric state is reached at a higher threshold. This threshold is considerably smaller than E_{c2} which is required to completely unwind the SmC_A^* phase as described in the previous section.

The SLS structure is favoured at low fields, as it requires only a small rearrangement in the $\tilde{\xi}_i$ of the layers from the field free helical structure. At intermediate fields, the competition between the field energy and the NNN interaction produces the compromise $2/3$ structure. Interestingly the soliton structure is recovered at higher fields, as the field energy now overcomes the NNN J_3 interaction. Clearly the $2/3$ structure is *field induced* while the comparable 2:1 structure of the Ising model is present even in the absence of the electric field [6] (see Fig. 2.4 and 2.5). However, the evidence for the latter structure was not found in the ellipsometric studies on freestanding films [23]. When J_1 is negative, the soliton structure is energetically more favourable than the $2/3$ structure at all fields till the unwound *ferro* phase is obtained at a high enough field. The same response is seen in the SmC_β^* and has been discussed by many authors earlier [44].

3.7.3 Structures in SmC_α^* phase

As the SmC_α^* phase occurs just below the SmA phase and the temperature range of stability of this phase is usually small for most of the compounds synthesized upto now, the tilt angle in this phase is quite small and also the influence of the field on the tilt angle (electroclinic effect) can not be neglected. Therefore, the experimental observations which depend on the tilt angle is quite subtle in this phase. In our calculations, we find that the soliton lattice structure is stable at low fields. As the field is increased beyond a threshold, a 4-layer periodic $2/4$ commensurate structure is stabilized as shown in Fig. 3.8c. This goes over to the unwound ferro structure at a higher threshold.

We will now calculate the apparent tilt angle θ_{app} corresponding to these field induced structures as a function of field to compare them with the experimental observations.

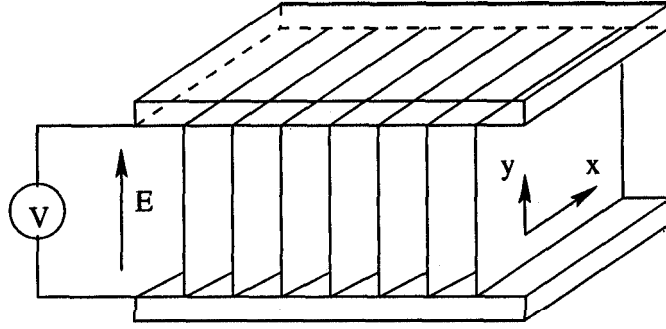


Fig. 3.9: The book shelf geometry of the sample. The flat smectic layers are perpendicular to the ITO coated glass plates and an electric field can be applied along the y-axis.

3.8 Calculation of apparent tilt angle

Consider the *book shelf* geometry of the sample in which flat smectic layers are perpendicular to the glass plates with the applied electric field \vec{E} in the plane of the layers and perpendicular to the bounding glass plates (along y-axis) as shown in Fig. 3.9. If we neglect the influence of the surface on the orientation of the director A , then at zero field due to the underlying helical structure, all the tilted phases are *optically uniaxial* with the optic axis along the layer normal (z-axis). As the field is increased this helical structure is deformed and the effective optical axis neglecting the small biaxiality of the medium for the present discussion, makes an angle θ_{app} with respect to the layer normal. This angle between the effective optic axis and the layer normal can be measured as a function of the field and is called apparent tilt angle θ_{app} . At high fields when the helix gets completely unwound it corresponds to the actual tilt angle made by the director A with the layer normal. As we have neglected the small biaxiality of the tilted smectic layers, θ_{app} is proportional to the average projection of the $\vec{\xi}$ vectors on to the in-plane electric field \vec{E} i.e., $\theta_{app} \propto \frac{1}{N} \sum_{i=1}^N \xi_{iy}$ where \vec{E} is along the y-axis. Hence we can calculate θ_{app} corresponding to different structures as a function of the field to compare with the available experimental observations as discussed below.

3.9 Results and comparison with experiments

The experimental variations of θ_{app} with the applied dc electric field obtained by Hiraoka et al. [14] in the ferroelectric and SmC_α^* phases for the compound MHPOBC are shown in Fig. 3.10 and Fig. 3.11. The corresponding theoretical variations of θ_{app} with electric field in different phases are shown in Fig. 3.12 and Fig. 3.13. It can be noted that the plateau at $\approx \theta/3$ observed experimentally in the ferroelectric phase is well reproduced. This plateau corresponds to the the field induced $2/3$ structure in the FI_L and FI_I phases in our model. It is also noteworthy that both in the field induced soliton structures of the ferriphases and the 4-layer $2/4$ structure in the SmC_α^* phase, θ_{app} is not a smooth function of the applied field. Experimentally also this non smooth behaviour is well known[6]. There are small jumps in θ_{app} as the field is increased and the location of these jumps depends on

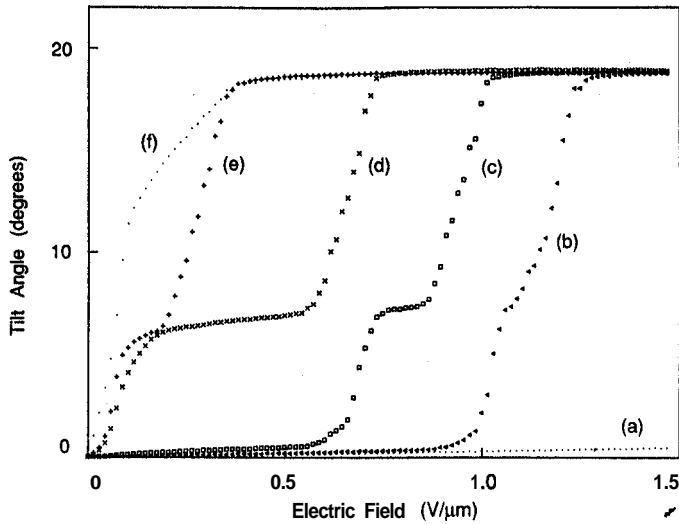


Fig. 3.10: Apparent tilt angle as a function of an applied electric field in SmC_A^* ((a) 113.0°C , (b) 114.7°C and (c) 115.2°C), SmC_γ^* ((d) 115.8°C and (e) 116.5°C), and SmC_β^* ((f) 116.7°C). Note the plateau at one third of the tilt angle in the ferrielectric phase. After Ref. [14].

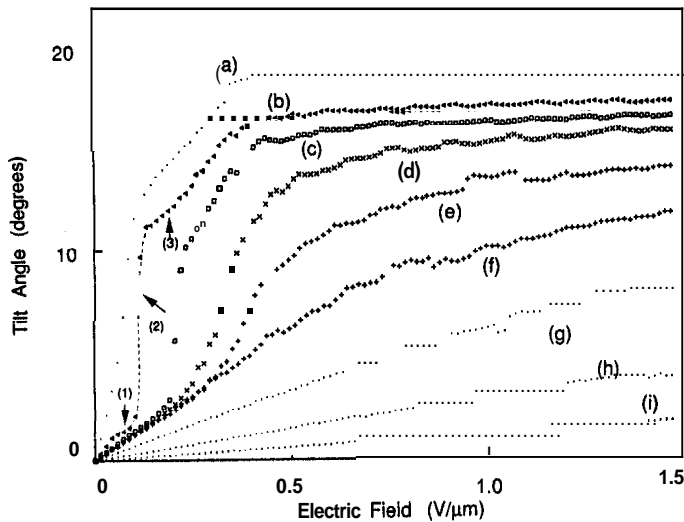


Fig. 3.11: Apparent tilt angle as a function of an applied electric field in SmC_β^* ((a) 116.8°C), SmC_α^* ((b) 118.2°C , (c) 118.5°C , (d) 118.8°C (e) 119.2°C and (f) 119.5°C) and SmA ((g) 120.0°C , (h) 121.0°C and (i) 123°C). Note the step like variation in the SmC_α^* phase. After Ref. [14].

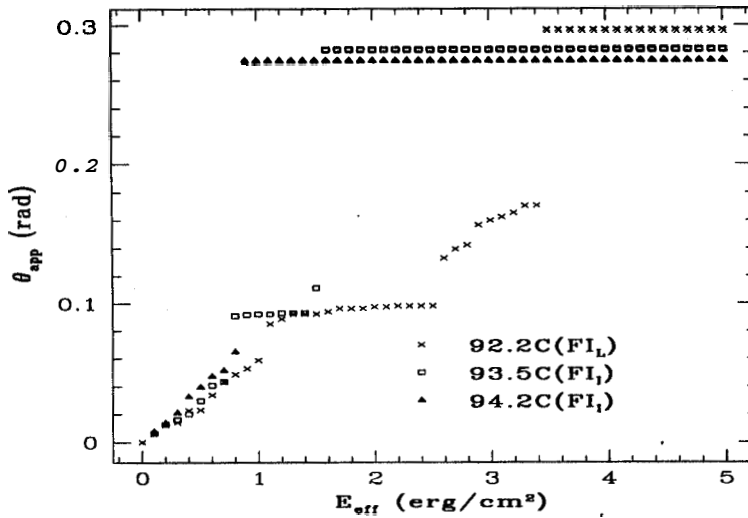


Fig. 3.12: Variation of θ_{app} with electric field at three temperatures corresponding to the **ferri** phases. Note the plateau at $\theta/3$ at the lower temperatures and the non-smooth variation in the high field soliton state at 92.2°C . Using $|\vec{P}| = 10^3$ cgs units, the physical field \vec{E} compares well with experimental data.

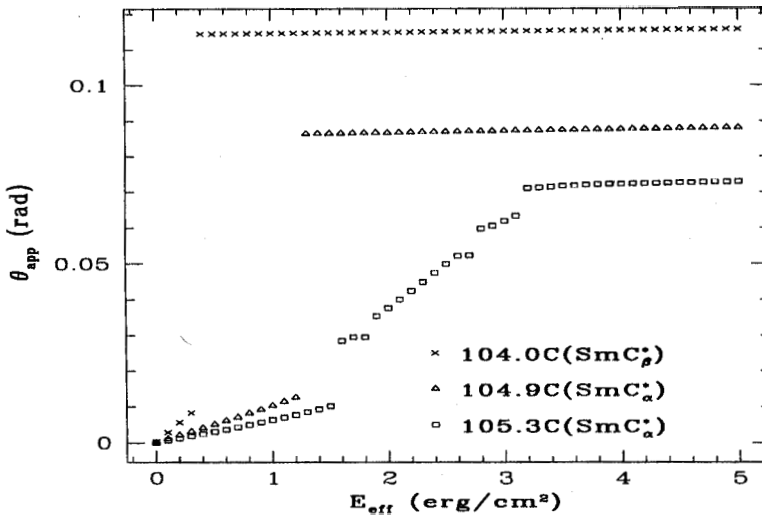


Fig. 3.13: Variation of θ_{app} with electric field in the SmC_β^* and SmC_α^* phases. In the SmC_α^* phase the variation is non-smooth for fields generating the $2/4$ structure. θ_{app} increases slowly with \vec{E} in the unwound state due to electroclinic effect.

the sample size used. As the phases on both sides of these jumps have soliton lattice, they have the same symmetry and the transitions between them can only be weakly first order in nature. Therefore these jumps may signify the possibility of field induced staircase often claimed from experimental observations in SmC_α^* and ferroelectric phases. However a detailed calculation to resolve this issue is beyond the scope of our present numerical technique. Further a detailed comparison of the calculated θ_{app} with the experimental data is not warranted for the following reasons: (a) It is well known that the walls have a very strong influence on the phase transitions exhibited by antiferroelectric compounds[48]. The wall interactions give rise to a non-uniform structure within each layer and in turn can produce a different type of staircase of *commensurate* and *incommensurate* helices[49]. (b) The dc electric fields used in the experiments can introduce other effects such as electric double layers which complicate the interpretation of experimental results.

3.10 Conclusions

In conclusion, we have made the first calculations on the effect of an electric field on the structures of different phases exhibited by antiferroelectric liquid crystals. We have also calculated the *apparent* tilt angles corresponding to these field induced structures. They agree closely with the experimental observations. It may be noted that the calculated structures are quite different from the *devil's staircase* of Ising spin variables which have been used in qualitative comparisons with field induced structures[6]. As we pointed out, even a simple chiral xy-model with only NN interactions produces a rich phase diagram as a function of field. In our model which incorporates an antiferroelectric NNN interaction, we have found a few low order *commensurate* structures. Our calculation is not exhaustive particularly in relation to higher order *commensurate* structures. It would be interesting to extend our calculations to look for such possibilities.